FFTF Scale-Model Characterization of Flow Induced Vibrational Response of Reactor Internals by J. A. Ryan and L. J. Julyk, United States.

ABSTRACT

As an integral part of the Fast Test Reactor Vibration Program for Reactor Internals, the flow-induced vibrational characteristics of scaled Fast Test Reactor core internal and peripheral components were assessed under scaled and simulated prototype flow conditions in the Hydraulic Core Mockup. The Hydraulic Core Mockup, a 0.285 geometric scale model, was designed to model the vibrational and hydraulic characteristics of the Fast Test Reactor. Model component vibrational characteristics were measured and determined over a range of 36% to 111% of the scaled prototype design flow. Selected model and prototype components were shaker tested to establish modal characteristics. The dynamic response of the Hydraulic Core Mockup components exhibited no anomalous flow-rate dependent or modal characteristics, and prototype response predictions were adjudged acceptable.

INTRODUCTION

Description of Fast Test Reactor

The Fast Flux Test Facility (FFTF) is located on the Hanford Reservation north of Richland, Washington, and is operated by the Westinghouse Hanford Company for the Energy Research and Development Administration. The central feature of the FFTF is the three-loop, sodium-cooled Fast Test Reactor (FTR), with a maximum power rating of 400 MWt. The primary purpose of FTR is to provide a high-intensity, fast-neutron flux (7×10^{15} n/cm^2-sec at 400 MWt) for irradiation testing of fuels and materials to be used in future fast breeder reactors. First full-power demonstration is scheduled for late 1979. Cutaway views of the FFTF plant and the FTR are shown in Figures 1 and 2a.

The core of the FTR is composed of a close-packed array of hexagonal driver fuel assemblies with interspersed control/safety rods and eight contact instrumented test positions located in a 'Y-shaped' pattern which divides the core into three 120-degree sectors. Peripheral positions within the reactor core are utilized for reflectors. The FTR core map is shown in Figure 2b.

Test assemblies fall into two categories: Open Test Assemblies (OTA's) which are cooled by the reactor cooling system and are distinguished from the basic driver fuel by an integral instrumentation package, and Closed Loop In-Reactor Assemblies (CLIRA's) which are cooled by independent sodium heat transport systems isolated from the reactor sodium environment. This isolation permits temperature, pressure, and flow conditions for testing fuel to failure with no radioactive contamination of the reactor sodium heat removal system.

Heat is extracted from the core by the flow of the sodium coolant (17.41×10^6 lb/hr) upward through the ducts, apportioned by orificing of the various assemblies, resulting in an average through-the-core coolant temperature rise of 300°F. The resulting flow of coolant discharges from the duct exit nozzles and flows upward past outlet plenum components, deflecting horizontally at or near the pool cover-gas interface, and then passes downward near the vessel wall toward the reactor vessel outlet nozzles.

Statement of the Problem

The occurrence of flow-induced vibrations could have adverse effects upon the FTR operations; there could be potential degradation of plant operational safety, structural integrity, or disruption of test sequences and programs. As a liquid metal cooled reactor, the FTR will generally operate at higher temperatures and flow-rates than previous water-cooled reactors. The combination of these factors tends to create a circumstance wherein potential vibration problems represent a departure from previous experience.

Definitive analytical predictions for potential flow-induced vibration problems in the FTR were not possible. The forcing functions are not readily definable, and the hydraulic flow channels are multiple and extremely complex. The most probable excitation mechanisms, in addition to random pressure fluctuations, include vortex shedding and self-excited vibration, both of which are nonlinear. Resonant frequencies and mode shapes of components and subassemblies tend to be analytically predictable; however, modal coupling, multi-degree of freedom system response, virtual mass effects of the liquid coolant, and damping in-situ are added unknowns which increase the complexity of analytical studies. Therefore, to promote safe, reliable FTR operation, the susceptibility of reactor internals to flow-induced vibrations was assessed by means of the Hydraulic Core Mockup (HCM) flow-induced vibration tests. This paper summarizes the HCM test program and details some of the more significant results.

Overview of the FTR Vibration Program for Reactor Internals

The objective of the FTR Vibration Program for Reactor Internals is to demonstrate the adequacy of the vibrational behavior of associated reactor internals. The on-going program consists of an overall reactor internals system vibration evaluation through HCM tests in combination with analytical

predictions, selected prototype vibration characterization tests, FTR vibration monitoring of selected components, and visual inspection of components for vibration-induced damage following discharge from the reactor.

Analytical predictions of the dynamic response of FTR internals in the outlet plenum were based on the assumption that vortex shedding would be the principal excitation mechanism. With the aid of an outlet plenum flow field characterization test, analyses of vortex-shedding and natural frequencies were carried out to establish that the vortex shedding frequency for each component was sufficiently separated from its natural frequency to ensure that no significant forced vibration would occur. Hydraulic flow testing in the HCM model was done to verify these analyses and provide increased confidence that the prototype will be free of detrimental vibrations.

The selected components for vibration monitoring in the FTR include an Instrument Tree (IT), Low Level Flux Monitor (LLFM), and the Vibration Open Test Assembly (VOTA). The dynamic response of each component will be monitored during non-nuclear isothermal preoperational testing for direct comparison with HCM results. In-vessel instrumentation in the IT and LLFM will be removed before power operations. However, the VOTA instrumentation will remain in place and will be intermittently monitored for three subsequent reactor cycles ($\sim$ 100 days per cycle) at power. As replaceable core components are discharged from the reactor, they will be inspected for evidence of undue impacting and/or wear.

HCM Objectives

Primary objectives of the HCM program were two-fold. First, to establish the vibrational characteristics of FTR internals under simulated FTR flow conditions, and to assess their susceptibility to flow-induced vibrations. A second objective was to confirm the design (from a flow-induced vibrational aspect) of FTR long-lead components or to establish the necessity of a design change, with the ability to conduct confirmatory tests on alternate designs. HCM tests were designed to provide the empirical basis for assuring the reliability of FTR internals. Simultaneously with the vibration program, a sequence of primary coolant hydraulic flow tests were conducted in the HCM, including measurements of velocities in the outlet plenum, mixing, pressure drop measurements, and gas entrainment.

HYDRAULIC CORE MOCKUP

General Description

The HCM was designed and fabricated as an isothermal 0.285 geometric scale model of the FTR. The model provided a simulation of both the vibrational and hydraulic characteristics. The model simulation included all hydrodynamically important wetted surfaces and all dynamically important masses, shapes, and stiffnesses of the FTR. Mechanical functions of the FTR were not modeled, but support conditions of components were simulated to provide the correct load paths and constraints.

Hydraulic flow channels, which represented potential sources of vibration excitation, were reproduced with the exception of the fuel, control, and reflector assemblies. Fuel pins were not included, but the hexagonal duct flow channels were simulated with tubing. The appropriately scaled pressure drops and flow distribution through and across the core was obtained by internal orificing of these simulated assemblies. The tubing was sized to obtain the correctly scaled stiffness with external weight added to obtain the appropriately scaled weight distribution. Scaled hex load pads were designed to permit simulation of core clamping. Component clearances were modeled in those areas where prototype clearances were judged to have an effect on component vibrational characteristics. Tolerances were modeled to a minimum of one mil (model dimension). Type 304 stainless steel was generally used for all components.

The HCM vessel was designed to operate at inlet pressures to 250 psig and internal temperatures of 250°F. The ability to operate at higher temperatures permitted evaluation of parametric variation of the fluid simulation. Maximum attainable flow through the vessel was 3700 gpm. Inlet and outlet piping were simulated to the second elbow.

The HCM facility did not simulate the FTR vessel support system. The HCM vessel was isolated from the steel frame, in which it was suspended, by six compression springs. The springs were sized to provide rigid body response in the vertical, pitch, and pendulum modes of 3 Hz or less. The factor of separation was at least 10 between the vessel rigid body modes and the minimum support frame modes.

Model Parameters

The similitude requirements for valid flow-induced vibration scale modeling of a structure in incompressible flow generally are well known[1]

and can be stated as follows (subscripts "m" and "p" refer to model and prototype, respectively):

$$\frac{(Re)_m}{(Re)_p} = 1, \text{ where Re is the Reynolds Number } (DU/\nu),$$

$$\frac{S_m}{S_p} = 1, \text{ where S is the Strouhal Number } (fD/U),$$

$$\frac{(\rho_s/\rho)_m}{(\rho_s/\rho)_p} = 1, \text{ where } \rho_s \text{ is the structural material density and } \rho \text{ is the fluid density, and}$$

$$\frac{\delta_m}{\delta_p} = 1, \text{ where } \delta \text{ is the log decrement damping factor.}$$

Additionally, the model and prototype must be geometrically similar and the ratio of elastic moduli, E_m/E_p, must be a constant for all points. From these dimensionless ratios the following can be stated:

$$\frac{y}{D} = \phi\left\{\frac{fD}{U}, \frac{DU}{\nu}, \frac{\rho_s}{\rho}, \delta\right\}$$

where y = vibration amplitude
D = characteristic length
U = flow velocity
f = natural frequency
ν = kinematic viscosity

For geometrically similar structures with the above four similitude ratios equal to unity, the scaling law between model and prototype is:

$$\left(\frac{y}{D}\right)_m = \left(\frac{y}{D}\right)_p$$

It is generally not possible to simultaneously satisfy all of these requirements; simultaneous simulation of Reynolds number and the structural Strouhal number is difficult at reduced scale.[2] Simulation of the Strouhal number was essential to the HCM tests, since distortion of the test results would occur with distortion of the Strouhal numbers.

The flow-vibration parameters for the HCM, based on the stainless steel model with water at 95°F and 250°F and a prototype with a sodium temperature of 1050°F, are given in Table 1. Based on these flow-vibration parameters, the scaling ratios between the model and prototype were established using the geometric scale factor of 0.285 and are included in Table 2. With the values of Table 2, the velocity ratio (model-to-prototype) must be 1.11 to achieve the requirement that the Strouhal number ratio be unity. That is, the ratio of model-to-prototype Strouhal number will be unity under the condition that the scaled HCM flow-rate is eleven percent greater than that of the prototype. Thus, 3700 gpm in the model scaled to 111% reactor flow-rate, or 3300 gpm scaled to 100% reactor flow-rate. Thus, for the HCM operating conditions, the Reynolds number simulation in the model was:

$$\frac{(Re)_m}{(Re)_p} = 0.122 \ (95°F)$$

$$\frac{(Re)_m}{(Re)_p} = 0.342 \ (250°F)$$

The effect of not simulating Reynolds number is primarily reflected in the Strouhal number simulation. This effect, in addition to the overall HCM simulation requirements, is discussed below.

Strouhal Number-Reynolds Number: Hydrodynamically induced vibration may be categorized as one of two types, forced or self-excited. The former would include the occurrence of vortices shed from a cylinder at or near the resonant frequency of the cylinder; the latter is of the type when motion of a cylinder would cause vortices to be shed synchronously at the frequency the cylinder is vibrating. The Strouhal number, relating the vortex shedding frequency to the cross-flow velocity and cylinder characteristic length, is a function of Reynolds number. Therefore, it is essential to know the effect of distortion of Reynolds number upon the Strouhal number to determine to what degree the HCM would simulate the FTR potential for vortex shedding forced vibrations. Generally, self-excited vibrations are less dependent upon Reynolds number as long as fully developed turbulent flow exists. This was the condition in both the model and prototype outlet plenum where the potential for self-excitation existed.

For Reynolds number in the regime of $80 < Re < 3.5 \times 10^5$, a single isolated cylinder subjected to cross-flow exhibits regular, well-defined vortex shedding, and the Strouhal number is essentially a constant over the

range of $500 < Re < 3.5 \times 10^5$. In this range the vortex shedding frequency is quite well-defined by $f_s = 0.21\ U/D$; whereas, for $Re > 3.5 \times 10^6$, the shedding frequency is given by $f_s = 0.27\ U/D$. In these two regimes, coincidence between the vortex shedding frequency, f_s, and structural natural frequency, f_n, can give rise to large lateral vibration amplitudes. In the regime $3.5 \times 10^5 < Re < 3.5 \times 10^6$, any shedding is irregular and the resultant structural vibrations are random. It is important, therefore, to identify the Reynolds number regimes of cross-flow across cylindrical components of the FTR and HCM.

Values of Reynolds number for the HCM and the FTR determined for the above conditions are given in Figures 5a and 5b as a function of the product of $(DU)_p$. Using the above-defined regimes of Reynolds number, three regimes of HCM simulation of the prototype vortex shedding are defined. These are identified as: FTR simulated, HCM conservative, and HCM unconservative. In the first range, vortex shedding coincidence occurring in the prototype would occur in the model. In the second range the model is considered conservative in that vortex shedding coincidence may occur in the model but not in the prototype. In the last range, the model is considered unconservative in that vortex shedding coincidence may occur in the FTR but not in HCM. FTR velocity profiles were experimentally measured[3] and from these data it was established that the HCM was operated in the first two regimes and not in the "HCM unconservative" regime.

Density Ratios: The ratio of density ratios, $(\rho_s/\rho)_m/(\rho_s/\rho)_p$ are 0.78 and 0.81 for 95°F and 250°F, respectively. Thus the effect of the virtual mass was somewhat greater in the model, yielding lower effective natural frequencies; the fluid excitation of the structure by the fluid was more effective in the HCM, yielding somewhat greater amplitudes. Both effects, although small, are considered conservative.

Damping: The HCM was designed to minimize structural damping. In general, this was achieved by designing all-welded HCM structural components and selective simplification of FTR design. Prototype mechanisms were not included in the model design; however, structural load paths and boundary constraint conditions were scaled and simulated. The effective damping, therefore, was designed to be less in the model than in the prototype, and the result would have been greater amplitudes of vibration in the model. With the minimization of effective damping, HCM model results were adjudged to be conservative.

Vibration Displacements: Since the deviations from correct modeling, as discussed above, were conservative, the relationship $(y/D)_m = (y/D)_p$ is considered to be conservative and HCM results are scaleable to the FTR.

HCM Configuration

Figure 3 is a view of the HCM model with key components identified. An illustration of the Hydromechanical Test Facility, in which the HCM was tested, is shown in Figure 4. As noted before, the HCM was configured to study the response of FTR components under scaled and simulated flow conditions; more specifically, to ascertain the susceptibility of the components to hydrodynamically induced vibrations. Table 3 tabulates the primary FTR components and Column 2 identifies the primary vibration design criteria used by the designer. The HCM, therefore, experimentally evaluated the response characteristics of those components whose primary vibration design criteria was specified as "vortex shedding."

The HCM pressure vessel essentially modeled the FTR reactor vessel wetted surface. A false head was designed at the appropriate plane, from which outlet plenum components were hung. The top head provided the pressure boundary, and along the vessel wall between these heads, all instrumentation leads originating from above the core support structure were exited through "pressure tight" fittings.

The major above-core (outlet plenum) components included in the model were:

- Instrument Tree (IT)
- In-Vessel Handling Machine (IVHM)
- Vortex Suppression Plate (VSP)
- Temperature/Liquid Level Monitor (T/LLM)
- Low Level Flux Monitor (LLFM)
- Closed and Open Test Assemblies (CLIRA and OTA)
- Control Rod Drive Line (CRDL)
- Thermal Liner

The primary components which constituted the inlet plenum/core region were:

- Core Support Structure (CSS)
- Core Barrel
- Fuel, Absorber, and Reflector Assemblies
- Radial Shielding
- Core Restraint

. Horizontal Baffle Plates
. In-Vessel Storage Module (IVSM)

Figures 6 through 18 show some of the model details as well as views of the HCM in the test stand.

Because of the 120° symmetry, essentially only components in a one-third sector of the HCM were instrumented to measure vibration. With respect to the instrumented Instrument Tree, only minor differences existed between it and the other two. These differences were primarily in the simulation of the Control Rod Guide Tubes (CRGT) and the Instrumentation Guide Tubes (IGT). The instrumented IVHM was a true geometric model of the prototype; geometric shape, stiffness, mass distribution, and boundary constraint were simulated. The remaining two IVHM's were primarily designed to simulate the wetted surface and hydraulic flow channels of the prototype.

Subsequent to the fabrication and initial assembly of the HCM, an LLFM was included in the model. One constraint on the modeled component was that it could not penetrate into the core region, but rather would have to be terminated at the core plane. To achieve an effective dynamic model, the design provided a clamped boundary condition at the false head, a prototypic bearing support at the inner horizontal baffle with scaled diametral clearance, scaled external diameter to satisfy the scaled Strouhal characteristic length, and added non-structural mass to provide scaled first mode resonant frequency. The correct ratio of the scaled vortex shedding frequency to the scaled first mode resonant frequency was thus maintained. The predicted forcing (vortex shedding) frequency in the model was below the first resonant frequency, and the effect of not scaling the higher resonances was considered acceptable.

The CRDL was tested in one core position only. The duct in that position was modified to allow insertion of a simulated absorber section (primarily mass). The drive line was a stiffness-mass simulation with external diameter scaled. Diametral clearances were scaled at regions of minimum clearance. The vertical position of the CRDL could be adjusted for testing from ten to one hundred percent of the withdrawn position.

The primary variations from prototypic scaling in the core region were: the ducts (as previously noted) and the absence of floating collars on the ducts. With respect to the fuel assemblies, full-scale water tests had been conducted on a prototypic fuel assembly.[4] This test sequence had studied the vibrational characteristics of fuel pins as well as the stability of a fuel duct with a floating collar. Thus, HCM data were not required for design verification of the fuel assemblies.

The passive mode of constraint was simulated by setting the restraint yokes at the Above Core Load Pads (ACLP) and the Top Load Pads (TLP) at the scaled across-core diametral gap. Under these constraint conditions, a variable degree of duct clamping was achieved. In some areas, bridging of ducts occurred permitting easy removal of core assemblies; other assemblies required significant force to extract them from the core.

The inlet nozzles were scaled as was the core basket. The flow channels were reproduced, and with the internal orificing of the ducts, the correctly-scaled across-core flow distribution was achieved. The outlet nozzles were geometrically scaled to provide the appropriately simulated flow conditions at the exit nozzles.

HCM TEST PROGRAM AND INSTRUMENTATION

Two separate vibration test sequences were conducted during the HCM operation. The first sequence consisted of the flow-tests and the second sequence was a series of shaker tests.

The flow-test sequence consisted of twelve discrete flow-tests plus several flow-sweeps. The discrete flow-tests were conducted at six model flow-rates from 1200 to 3700 gpm (36% to 111% scaled reactor flow). Flow-sweeps were conducted between the six discrete flow-rates. Test temperatures were 95°F and 250°F.

Internal vibration instrumentation consisted of accelerometers. Two types were used; the first, a miniature biaxial piezoresistive unit was used where orthogonal measurements were required, and the second was a uni-axial piezoelectric unit. The biaxial accelerometer was critically damped and had a flat response from d.c. to 1200 Hz. The crystal accelerometer response was flat from 5 Hz to 5000 Hz. All internal accelerometers had quarter-inch, hard-line cable of sufficient length to exit from the vessel. The crystal accelerometer had an extremely low case sensitivity to pressure fluctuation while the biaxial units were insensitive to pressure fluctuation.

Accelerometer locations are schematically shown in Figure 19. Each accelerometer was provided with a unique identification number which was used for identifying all recorded and analyzed data.

The Vibration Data Acquisition System (VDAS) consisted of signal conditioners, two sets of fourteen variable gain amplifiers patched into two

fourteen-channel FM tape recorders. All accelerometer sensitivities were normalized to 110 Mv/g. The output of all accelerometers was recorded on tape in prescribed data sets for permanent record and post-test analysis. As vibration signals were recorded, they were displayed on monitor scopes for qualitative evaluation and detection of potential impacting.

The data analysis was primarily accomplished with a real time analyzer. The analyzer was operated in series with an ensemble averager and the spectral output was the result of an ensemble average of N statistically independent spectrum samples. The value of N was selectable and noramlly set at 32 or 64. The ordinate value of the spectral output of the ensemble averager was proportional to $Mv/\sqrt{Hz}$; thus the ordinate scale of the Power Spectral Density (PSD) plots has units of $g/\sqrt{Hz}$.

A series of wet and dry shaker tests, utilizing sinusoidal swept-frequency excitation, were performed in-situ on the following head-hung components:

- Instrument Tree
- IVHM
- CLIRA
- OTA
- LLFM
- T/LLM
- VSP

Where space permitted, a small portable exciter was attached to each component above the VSP to excite the component both wet and dry from the same location. The IVHM, CLIRA, and OTA were not accessible at the above location and therefore were excited above the false head on the support standpipe. The VSP was not directly excited, but data were taken during sweeps on other components.

Sinusoidal excitation from 10 to 200 Hz was applied with the exciter through an impedance head. The force signal was routed through the shaker servo-control to provide constant force frequency sweeps. Component response was measured with the same accelerometers and locations used during flow-tests. Data were recorded on the VDAS with all accelerometers normalized to 110 Mv/g. Subsequent data reduction consisted of Co-Quad (Cross Power Spectral Density) plots displaying the product of excitation force and response acceleration versus frequency. Resonant frequency, damping and mode shapes were extracted from the Co-Quad plots.

TEST RESULTS

The initial results of the flow-tests confirmed pre-test predictions that components subjected to fluid excitation would respond at their natural frequencies. The fluid excitation is broad band and contains energy over a large frequency spectrum. Long, slender components with well-defined resonances, such as the LLFM and CLIRA, exhibited distinctive response at their natural frequencies (see, for example, Figures 32 and 36). However, no occurrence of synchronous vortex shedding with component natural frequency was observed on any component over the entire range of flow-rates. Typical responses of a component as a function of flow-rate are shown in Figures 40 and 41. The displacements are the vectorial sum of the orthogonal values as calculated by numerically doubly integrating the acceleration PSD's.

Large outlet plenum components, such as the Instrument Tree and the IVHM, did not exhibit well-defined modes of response. The flow paths through and around these components gave rise to multiple locations of excitation as well as multiple types of excitation; cross-flow, and parallel flow. Fluid excitation existed on the primary structure as well as the various sub-structural components.

Typical measured response of the Instrument Tree and the IVHM are shown in Figures 20, 21, 24, and 25 as generated at 3700 gpm. From these PSD plots and further analysis of the tape data, "mode shapes" were calculated for the observed resonant response of the Instrument Tree and IVHM. Tracking filters were set to track at the desired center frequency and the filtered output of the recorded data was displayed on a dual channel oscilloscope. By referencing all accelerometer output to a "common accelerometer" output, amplitude and phase data were measured. The results of this procedure are tabulated in Tables 4 and 5.

Subcomponent response on the Instrument Tree was measured on the CRGT and IGT. From the measured response of these components (see Figures 22 and 23), not only is response apparent at the component natural frequency, but Instrument Tree main frame response is observable. For example, the Instrument Tree "out-of-plane" bending mode of 51 Hz was measured on the output of IGT accelerometer (Figure 23). The location of this accelerometer was such that it sensed not only lateral motion of the IGT but also out-of-plane Instrument Tree motion.

Three segments of the VSP were instrumented to measure plate bending motion (vertical motion). A typical response of one segment is shown in Figure 26. The strong response at 150 Hz was identified as the first plate bending mode of the segment. To evaluate the effect of the virtual mass of the coolant upon the VSP, a series of tests were run at various pool heights and at a flow rate of 3100 gpm. Three conditions of pool height are shown; normal pool height, pool height at the VSP, and pool height six inches below the VSP (see Figures 27, 28, and 29). The shift in the first plate bending mode can be seen to increase from 150 Hz to 185 Hz as the liquid level is lowered. With the pool height below the VSP, no direct fluid excitation of the plate segment existed. The response is entirely due to coupling of the VSP segment with adjacent head-hung components through the false head by means of the VSP hanger supports.

One VSP segment adjacent to the thermal liner had a small unsupported tab. During flow-tests, this tab segment exhibited a scaled prototype frequency response below 20 Hz. This was below the minimum acceptable frequency for prototype VSP response. The tab was removed and subsequent tests indicated the increase in minimum scaled prototype frequency was above the 20 Hz minimum limit. This fix was deemed acceptable and incorporated in the FTR design.

CRDL impacting was observed during flow-tests at the interface region of the dashpot and the driveline. The upper driveline was subjected to cross-flow in the region above the CRGT and the VSP in addition to parallel flow in the CRGT. Calculations of the lateral motion of the driveline indicated that the peak displacement amplitude of vibration was greater than the nominal diametral clearance between the driveline and the dashpot. This lateral motion was therefore contributory to the impacting observed. However, the amplitudes of the measured impact were significantly greater than those that could be calculated using the measured driveline response data. Typical lateral motion of the driveline is shown in Figures 30 and 31. During the pool height variation tests conducted on the VSP, the pool height was below the top of the CRGT and no cross-flow existed on the upper driveline. Impacting was still observed at the same location, only slightly reduced in amplitude, thus indicating the parallel flow inside the CRGT was the primary flow contributing to the impacting.

The mechanism of impacting was concluded and demonstrated to primarily involve differential lifting of the dashpot from the dashpot seat in the CRGT due to the hydraulic lifting forces generated by the pressure drop across this restriction. The dashpot was essentially lifting and tilting laterally and impacting the driveline. Post-test examination of the CRDL substantiated the above conclusions.

The CRDL had been simulated to initially assess driveline response to cross-flow excitation. Since impacting was demonstrated to be a function of internal parallel flow in the CRGT, the modeling was reviewed to more correctly predict impacting potential in the FTR. It was established that the simulation could be improved by more correctly scaling the model-to-prototype dashpot weight-to-hydraulic lifting force ratio. Also, the model CRGT flow had been higher than the correct scaled flow due to FTR design changes which had occurred after model fabrication. In reduced scale model tests components, for which gravity is the primary restoring force, will chatter at lower scaled velocities; thus, the higher scaled flow resulted in further distortion.

Subsequent tests showed that more correct scaling of the dashpot simulation and the CRGT flow resulted in significant decreases in impact amplitude. This reduction, in combination with redesign of the interface between the dashpot and driveline, were adjudged acceptable for FTR operation.

Two CLIRA positions were instrumented. In core position 1202, there was apparent bridging occurring in the core and the degree of core clamping was less than in position 1406. The measured response indicates a lower first mode response for core position 1202, 30 Hz as compared to 44 Hz in position 1406 (see Figures 32 and 33). Pretest model analytical predictions, which considered fully-effective core clamping, agree quite well with the measured response at position 1406.

Argonne National Laboratory supported the post-test analysis of HCM data. One area of effort was the comparison of predicted response of HCM components with the measured response. For a slender circular component of well-defined boundary conditions such as the CLIRA in position 1406, the agreement between predicted/measured response was within a factor of two.[5]

CLIRA 1406 was instrumented both in the outlet plenum and in-core region. Response data are shown in Figures 34 and 35, respectively. The first mode response at 44 Hz is barely discernible from the in-core measured response. The measured CLIRA in-core response is more similar to the in-core response measured on a typical driver, 1404. Two accelerometers were installed on this driver; accelerometer 13-1404 was installed at the center of the core, and accelerometer 14-1404 was installed in the plane of the TLP (see Figure 19b). Comparison of 27-1406X with 13-1404X and 14-1404X (Figures 35, 38, and 39)

shows similar PSD characteristics. These response characteristics were quite similar to those measured from other instrumented driver and reflector assemblies.

The LLFM simulation, as previously described, scaled the geometric shape of the prototype LLFM in the outlet plenum and its corresponding first natural frequency. The model component was designed and analyzed to have a wetted first mode response in-situ of 30 Hz. Figure 36 shows the measured response at 3700 gpm with a dominant first mode response at 31 Hz. Damping, as calculated using the "half power point" from the PSD plots gave values of about 2%. The calculated displacements as a function of flow-rate are shown in Figure 40.

The Core Support Structure could potentially be excited by the turbulent mixing occurring in the inlet plenum in addition to flow-excitation. Accelerometer 2Y was mounted on the CSS to measure vertical response. Typical measured response is shown in Figure 37, essentially a flat spectral response. This response form was constant over the range of flow-rates tested. The data indicated no definite forced response due to turbulent mixing or other flow-excitation. Lateral accelerometers mounted on the CSS showed the same spectral response shape.

Tests conducted at 250°F yielded essentially the same results as those conducted at 95°F. No significant variation was observed in amplitude of component response, nor in the frequency content of response. A series of tests were conducted with two- and one-loop outlet plenum flow. At equivalent flow-rates, no significant differences were detected in the measured outlet plenum responses. Some reduction in amplitude was measured on components located near the outer wall (thermal liner) where the flow-rate was less.

The results of the "wet" shaker test modal survey of the outlet plenum components were confirmatory to the flow-test modal identification. Tables 6 and 7 compare the results of the "wet" shaker tests on the Instrument Tree and IVHM with the flow-test results. The resonant frequencies identified in both tests agreed quite closely; however, differences existed in the majority of the mode shapes. The source of excitation during the shaker tests was located on the IT and IVHM at a single point (internal on the IT column, external on the IVHM support), whereas during flow-tests these components were subjected to multiple point excitation. Of particular interest, however, is the close agreement in several of the mode shapes; for example, the 49 Hz Instrument Tree mode.

One IVHM mode could not be reproduced during the "wet" shaker tests. This was the 12.5 Hz mode. Only one exciter location was available for the shaker tests and from this location, the mode could not be "tuned in." There were indications from some Co-Quad plots that the mode may have been responding, but the amplitude was exceedingly low. Fundamental frequencies and damping values, obtained from shaker tests on "dry" and "wet" components, are given in Table 8 for several outlet plenum components.(6)

Only one reactor component was shaker tested with near prototypic boundary constraints, an engineering mock-up of the Instrument Tree. The primary purpose of this test was to characterize the IGT's. Since the test was conducted at room temperature, correction for frequency due to the variation in properties at temperature was estimated as 0.9. Converting the measured resonant frequency to reactor operating temperature resonant frequency and ratioing these values with the model test results, f_m/f_p, gives a measured model scale factor. For several IGT, the model scale factor varied from 3.37 to 4.10, compared to a designed value of 3.88. The CRGT scale factor was calculated at 3.83. Main frame Instrument Tree model scale factors varied from 2.5 to 5.0; the lower values were generally associated with IT torsional modes and the high values with IT bending modes. The HCM IT did not model the mechanical details of the prototype IT, such as operating mechanisms. These mechanisms would tend to produce nonlinear response in the IT due to gear meshing and backlash. The shaker test results indicated the IT response to be nonlinear for the low forcing amplitude applied.

CONCLUSIONS

The HCM tests, in conjunction with the prototype component tests, are considered confirmatory of the adequacy of the vibrational characteristics of the FTR internals. Over the range of flow-rates tested, no unstable flow rate dependent resonant or forced response was observed. Outlet plenum component resonant response was observed; however, the response amplitudes increased as a function of increasing flow and no anomalous response disproportionate to flow increment was observed. In-core component response was generally low amplitude and highly damped.

Based upon measured model flow-velocities, it was established that the operational range of HCM flow-tests were never in the unconservative region of the HCM/prototype vortex shedding relationship (see Figures 5a and 5b). HCM flow-tests at 95°F and 250°F did not show significant differences in

measured response. Considering these results, it has generally been concluded that scale model tests of the HCM type can be conducted at the lower temperature, thereby simplifying the model vessel design requirements.

Analytical predictions of model response agreed more closely with response measurements on the more simple components, such as CLIRA, which had well-defined modes. The assumptions made as to the location of the dominant vortex shedding, boundary conditions, etc., tended to be critical in obtaining accurate analytical predictions. In the limited number of cases where prototype components were dynamically tested, the agreement with model flow-test and shaker tests was generally good.

Scale model tests can be an effective method of complementing prototype analysis and test to ensure reliable, vibration-free reactor operation. By starting model design concurrently with reactor design, vibration characteristics of long-lead reactor components can be established in time to have an input into the final design and fabrication. The design and testing of a model of the complexity of the HCM imposes stringent requirements for the simulation of each component and the need to understand the vibration environment in which it will be operating. For example, where gravity is the primary restoring force, accommodations must be made in the model to account for this effect. When the model program is carefully planned and executed, it can be concluded that gross vibrations occurring in the model may also occur in the prototype; conversely, the absence of gross vibrations in the model increases the confidence in the adequacy of the reactor design. The general conclusion from the analytical and experimental program is that no gross vibrations should arise during planned FTR operations. Table 3 is a summary of these results.

However, accurate flow-induced vibration predictions in a complex fluid/structure system such as the FTR are not amenable to current analytical methods. Although physical modeling offers the greatest potential for studying the flow-induced response, it too is an approximation and requires careful analytical and experimental techniques to eliminate uncertainties and account for model distortions. Hence, in an effort to guard against potentially unpredicted results and to verify the HCM results, selected components will be instrumented for in-vessel vibration monitoring in the FTR.

ACKNOWLEDGEMENTS

The HCM program involved several years for planning, designing, fabrication, testing, and analyzing results. The authors wish to acknowledge the many people who gave so freely of their time, direction, and insight over the course of the program. To those Engineers and Scientists from ERDA-FFTFPO, HEDL, WARD, and ANL, who were associated with the program from conception to execution, must go a great share of the credit.

REFERENCES

1. Vickery, B. J., and Watkins, R. D., "Flow-Induced Vibration of Cylindrical Structures," Hydraulics and Fluid Mechanics, R. Sylvester, Editor, McMillan Company, 1964.

2. Trent, D. S., "Applications of Geometric Models for the FFTF Hydraulic Core Mockup," BNWL-575, November 1967.

3. Polentz, L. M., Ballard, D. L., and Nunamaker, F. H., "FFTF Outlet Region Feature Model Localized Pool Velocities," HEDL-TME 71-48, December 1971.

4. Kinsel, W. C., "Flow-Induced Vibrations of Spiral Wire-Wrapped Fuel Assemblies," presented at ASME Winter Annual Meeting, December 1975.

5. Tarula, P., "Comparison of Analytical Predictions with HCM Test Results for FFTF Reactor Flow Induced Vibrations and Summary of Prediction Methods," ANL-CT-76-31, April 1976.

6. Ryan, J. A., Simmons, M. D., and White, R. G., "FTR HCM Scale-Model Shaker Tests," HEDL-TME 75-97, September 1975.

FAST FLUX TEST FACILITY

WestinghouseHanford

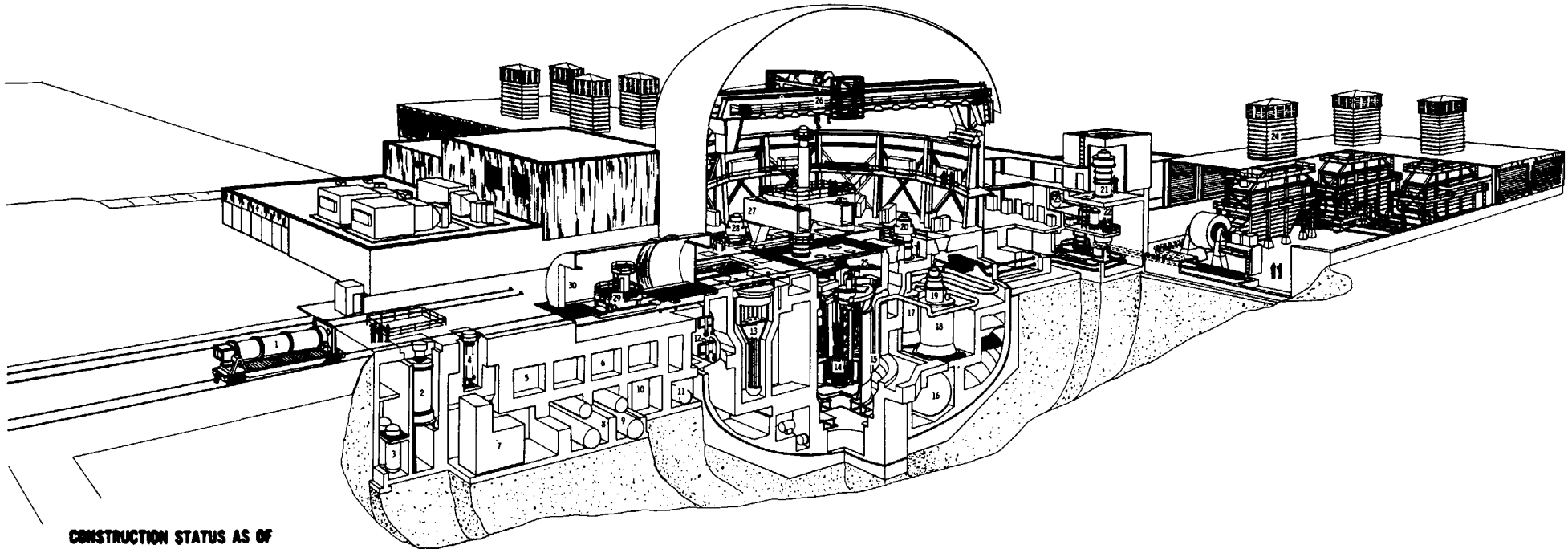

CONSTRUCTION STATUS AS OF

LEGEND

- COMPONENTS INSTALLED
- COMPONENTS ONSITE NOT INSTALLED
- COMPONENTS AT HTSF
- CONSTRUCTION COMPLETE

1. MAINTENANCE CASK
2. LMFBR CASK LOADING STATION
3. LIQUID NITROGEN DEWARS
4. SODIUM REMOVAL STATION
5. RAPS GAS COMPRESSOR CELLS (ONE COMPRESSOR EACH CELL)
6. CAPS GAS COMPRESSOR CELLS (ONE COMPRESSOR EACH CELL)
7. RAPS* COLD BOX ASSEMBLY
8. RAPS* TANK CELL
9. CAPS** TANK CELL
10. CAPS** COLD BOX ASSEMBLY

*RAPS RADIOACTIVE ARGON PROCESSING SYSTEM

**CAPS CONTAMINATED ARGON PROCESSING SYSTEM

11. RECYCLE COVER GAS STORAGE VESSEL
12. INTERIM EXAM AND MAINTENANCE (IEM) CELL
13. INTERIM DECAY STORAGE (IDS)
14. REACTOR
15. REACTOR GUARD VESSEL
16. PRIMARY SODIUM STORAGE VESSEL T-43
17. PRIMARY PUMP GUARD VESSEL
18. INTERMEDIATE HEAT EXCHANGER GUARD VESSEL
19. INTERMEDIATE HEAT EXCHANGER HTS #2
20. PRIMARY SODIUM PUMP HTS #2
21. SECONDARY PUMP
22. SECONDARY PUMP GUARD VESSEL
23. SECONDARY SODIUM EXPANSION TANK
24. DUMP HEAT EXCHANGER
25. HEAD ACCESS COMPARTMENT
26. POLAR CRANE
27. CLOSED LOOP EX-VESSEL HANDLING MACHINE (CLEM)
28. PRIMARY SODIUM PUMP HTS #1
29. BOTTOM LOADING TRANSFER CASK (BLTC)
30. EQUIPMENT AIRLOCK

Figure 1. FFTF Cutaway View

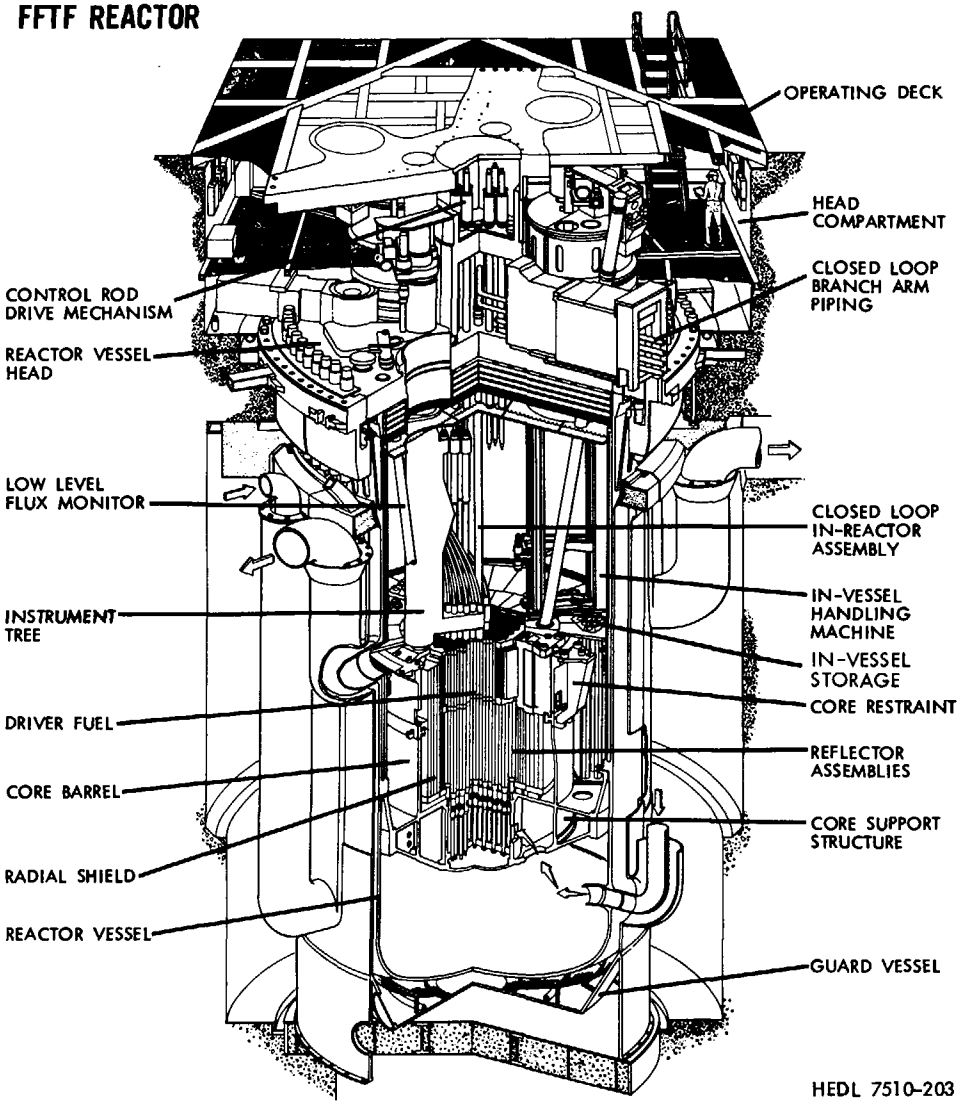

Figure 2a. Reactor Vessel and Internal Components

CORE MAP WITH LATTICE IDENTIFICATION

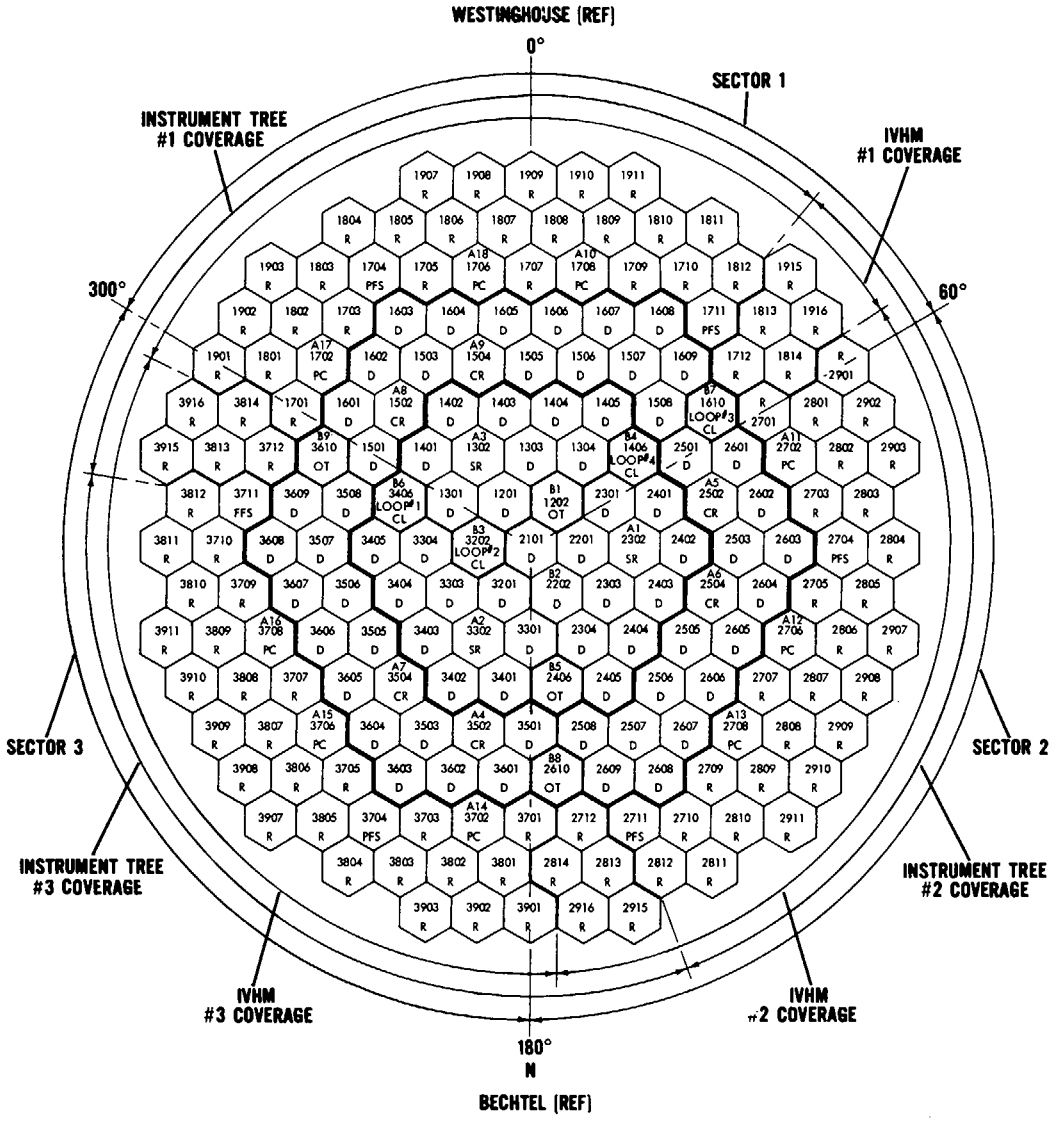

LEGEND

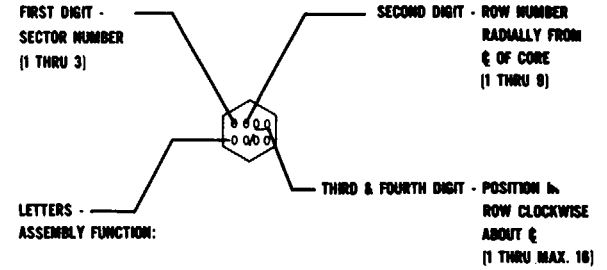

- CL CLOSED LOOPS-4
- OT OPEN TEST ASSEMBLIES-4
- D DRIVER POSITIONS (29 INNER (ROWS 1 THRU 4); 45 OUTER (ROWS 5 & 6))
- SR SAFETY RODS-3
- CR CONTROL RODS-6
- PC POTENTIAL FIXED SHIM OR MOVABLE PERIPHERAL CONTROL RODS-9
- PFS POTENTIAL FIXED SHIM LOCATIONS-6
- R REFLECTORS-93 TO 108 (ROWS 7-9)
- REACTOR CAPABILITY-6 CLOSED LOOPS

REACTOR VESSEL HEAD PENETRATIONS (REF)

- A1-A3 SAFETY RODS-3
- A4-A9 CONTROL RODS-6
- A10-A18 POTENTIAL FIXED SHIM OR MOVABLE PERIPHERAL CONTROL RODS-9
- B-1 OT
- B-2 D
- B-3 LOOP 2 CL
- B-4 LOOP 4 CL
- B-5 OT
- B-6 LOOP 1 CL
- B-7 LOOP 3 CL
- B-8 OT
- B-9 OT

Figure 2b. Core Map with Lattice Identification

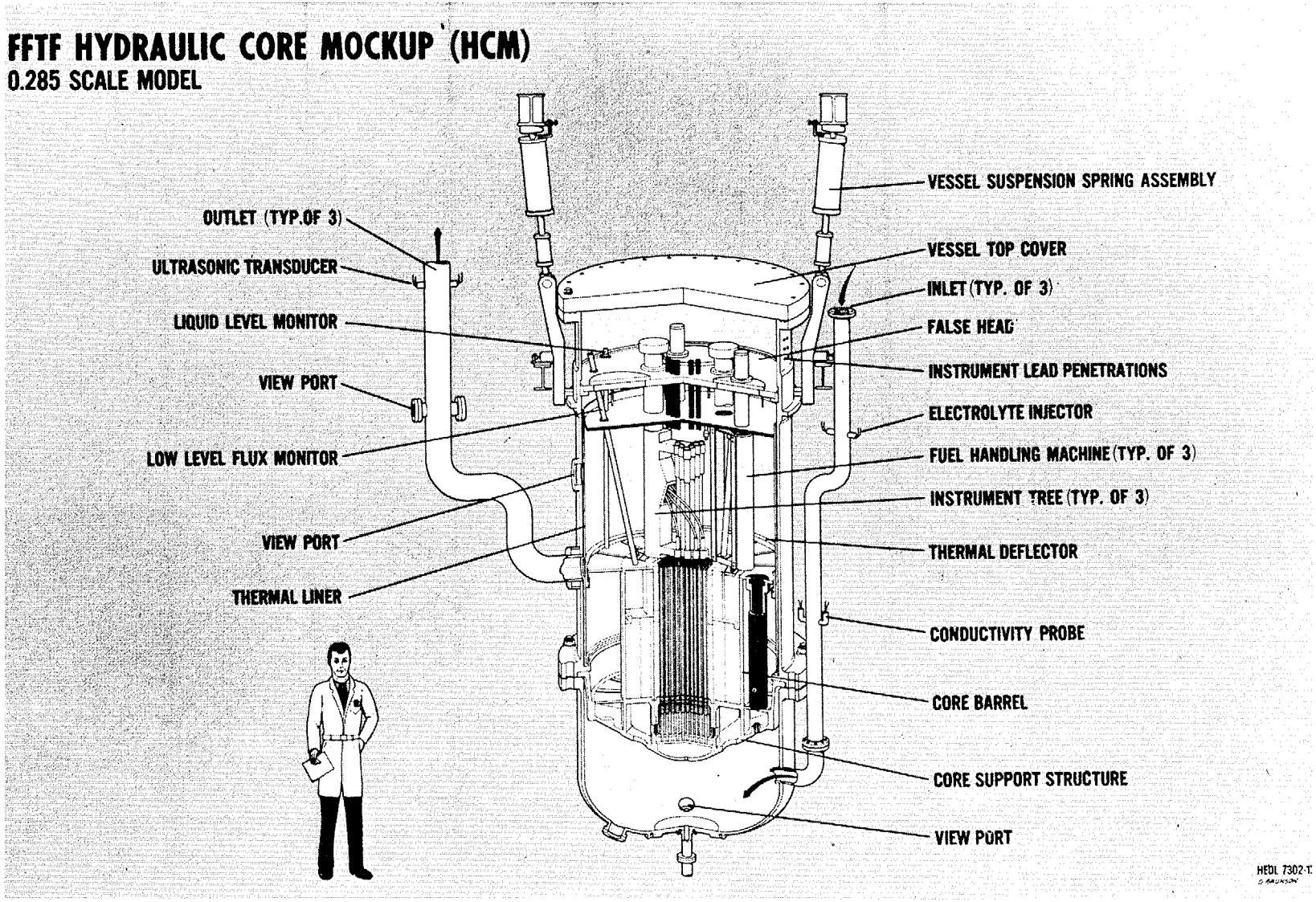

Figure 3. FFTF Hydraulic Core Mockup

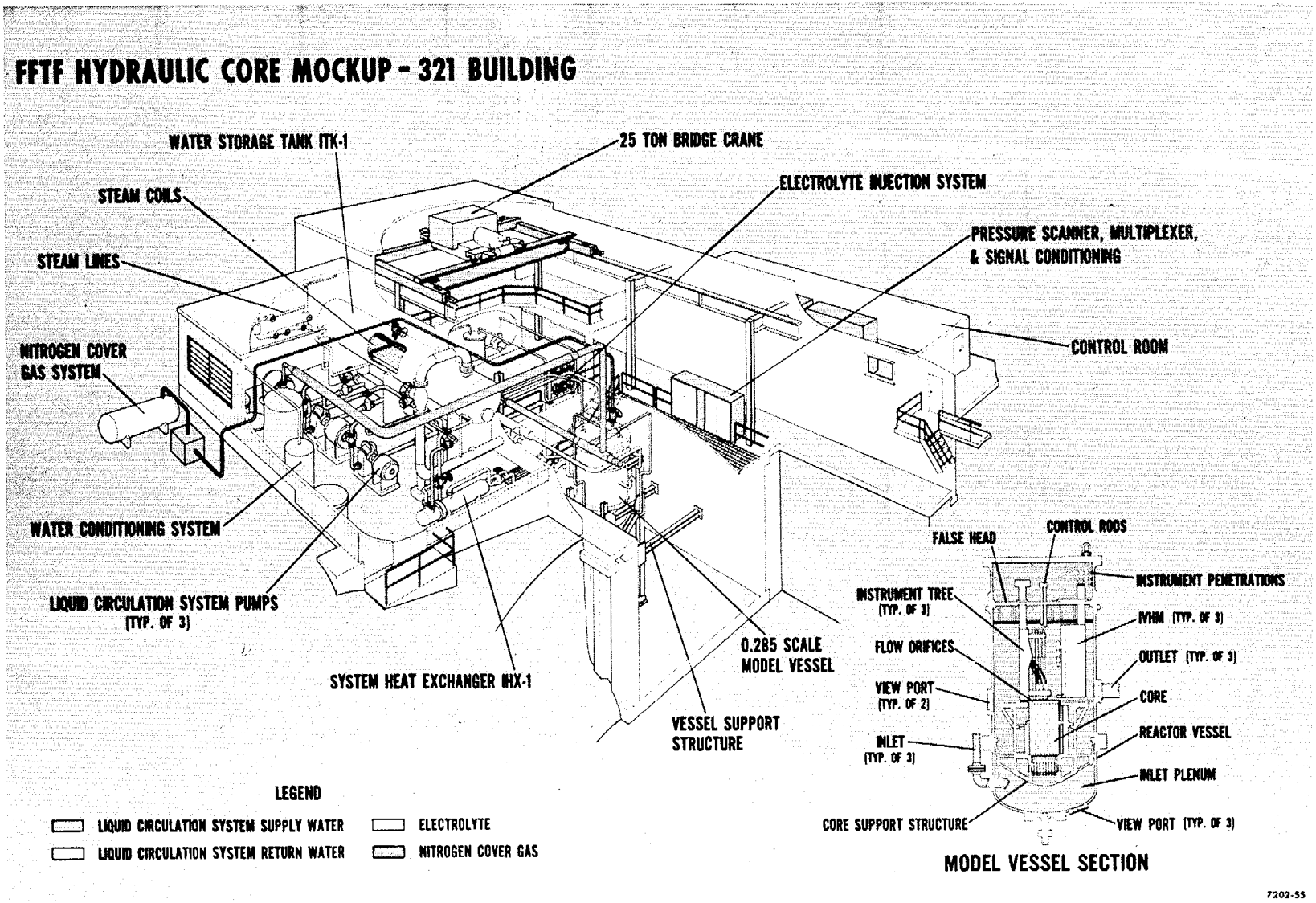

Figure 4. FFTF Hydraulic Core Mockup - 321 Building

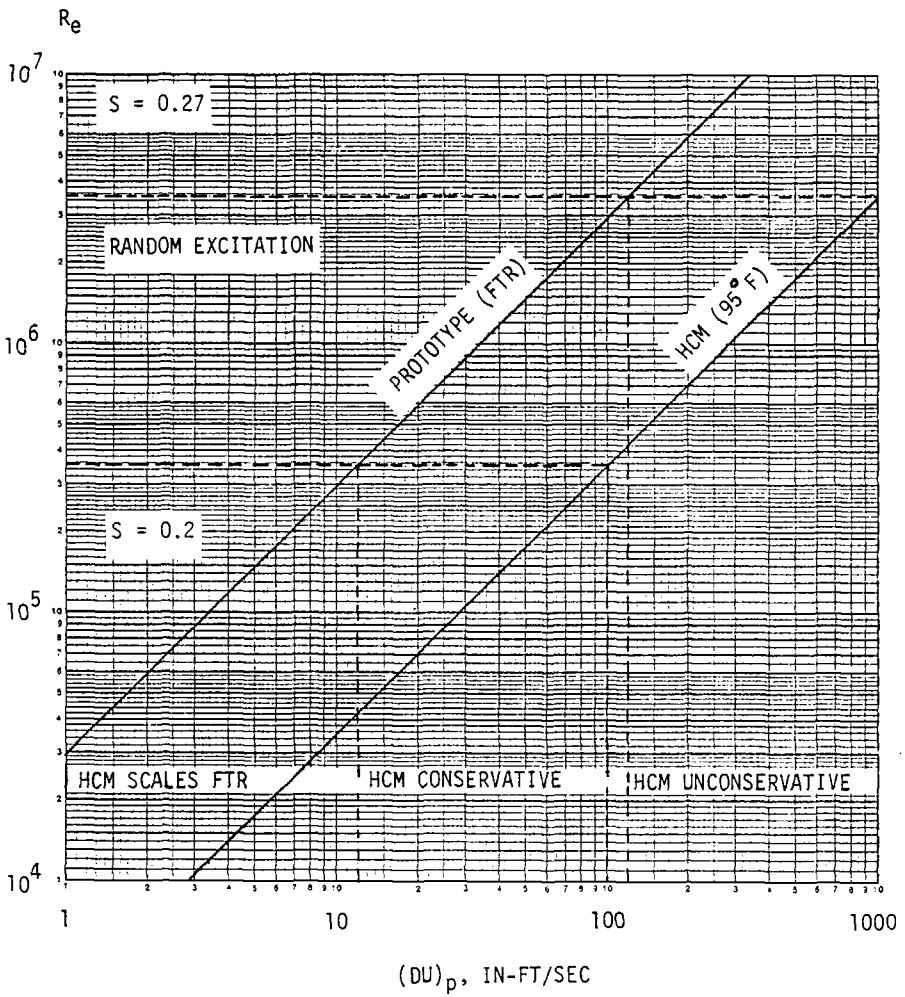

Figure 5a. HCM/Prototype Vortex Shedding Relationship (95°F)

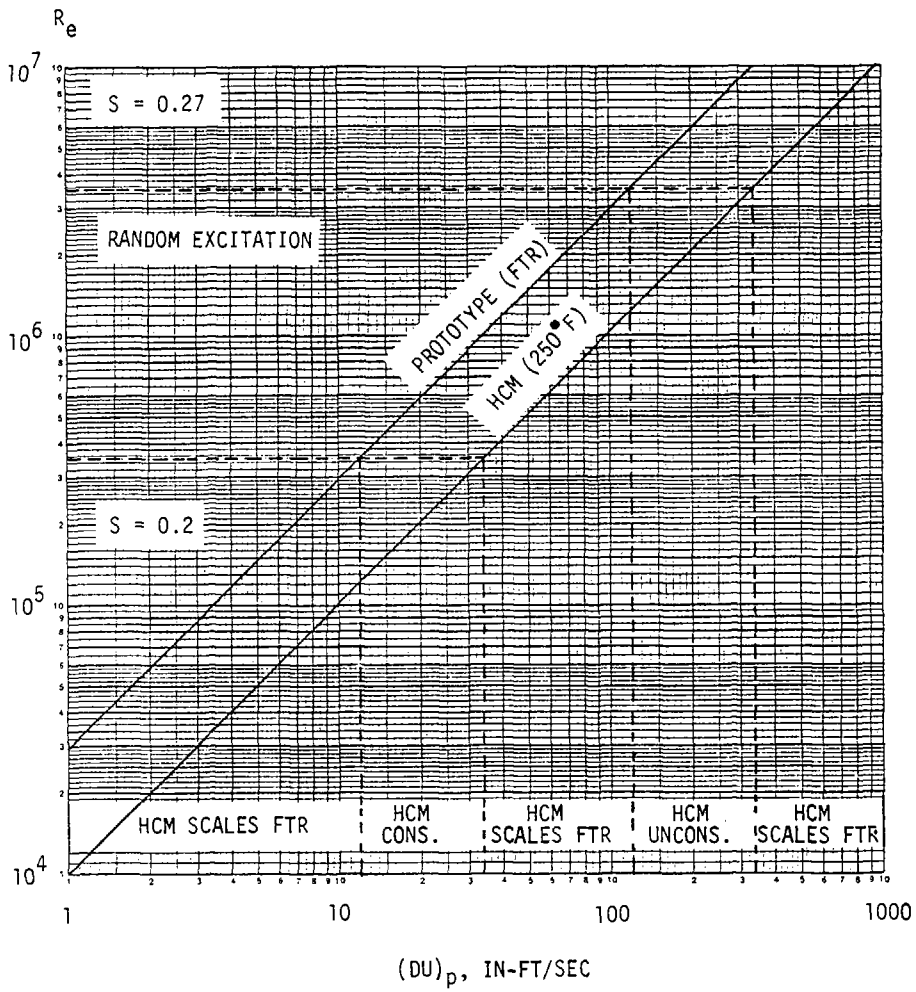

Figure 5b. HCM/Prototype Vortex Shedding Relationship (250°F)

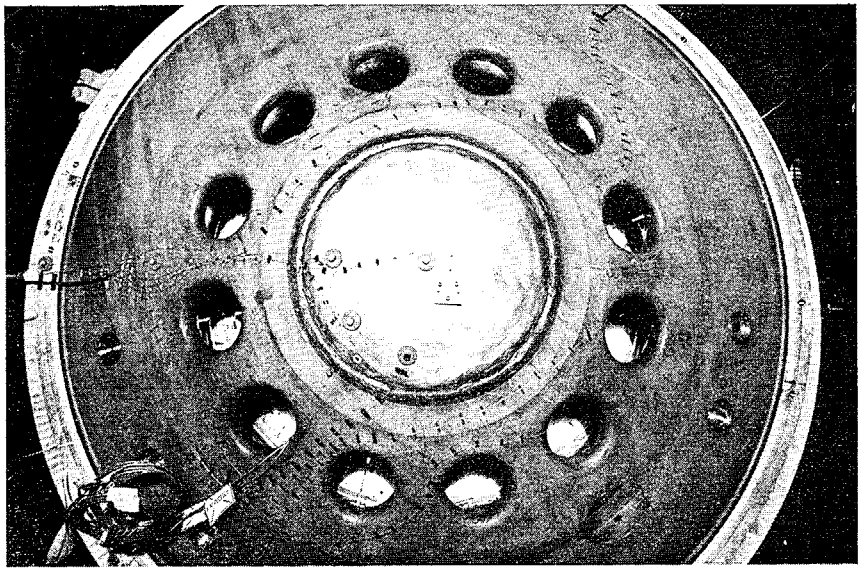

Figure 6. Bottom View of Core Support Structure

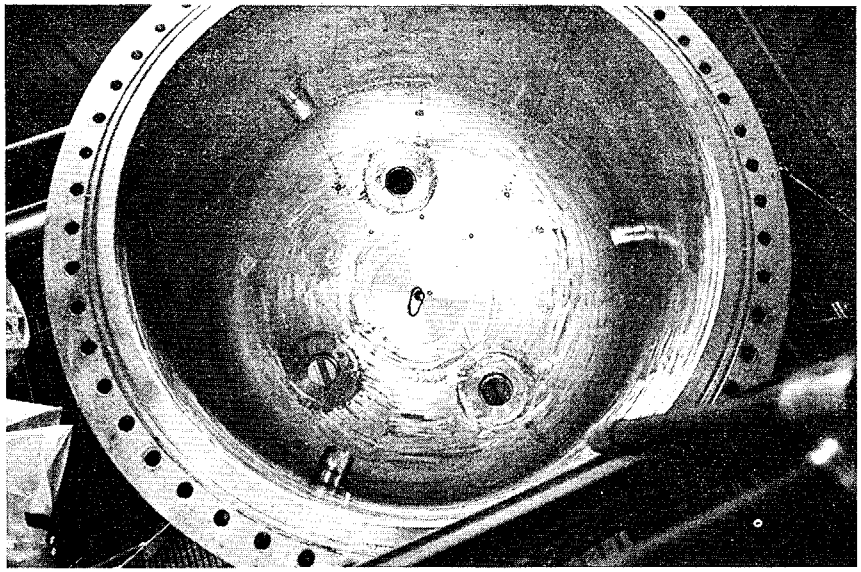

Figure 7. Inlet Plenum

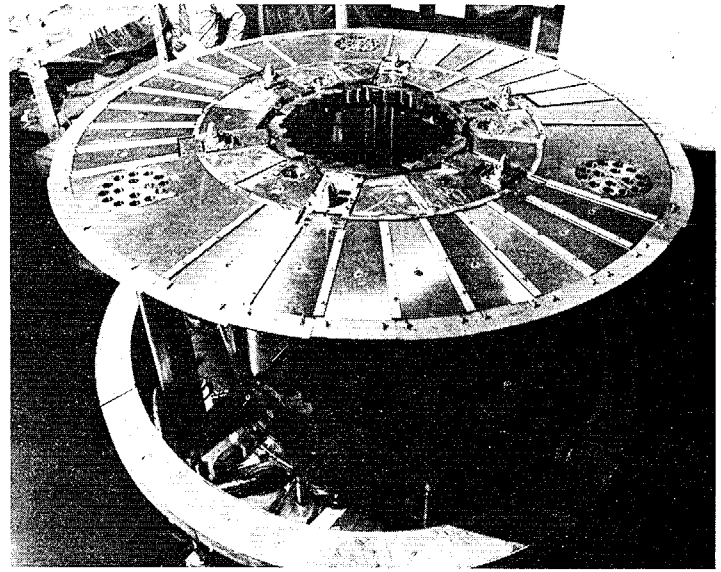

Figure 8. Overall View of Core Assembly

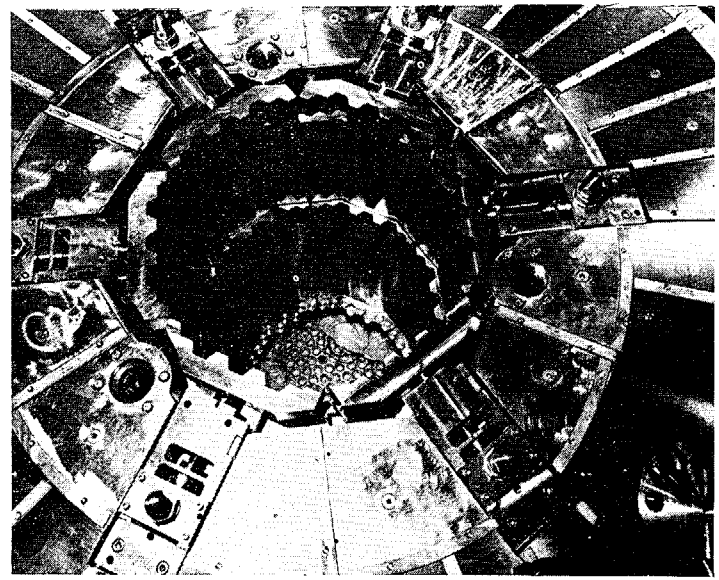

Figure 9. Top View of Core Assembly

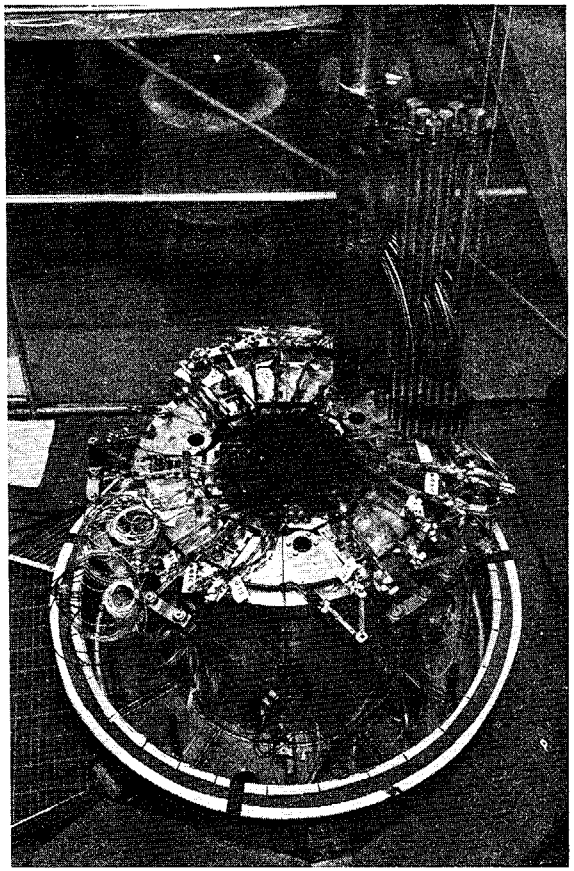

Figure 10. Core Assembly Fit-up

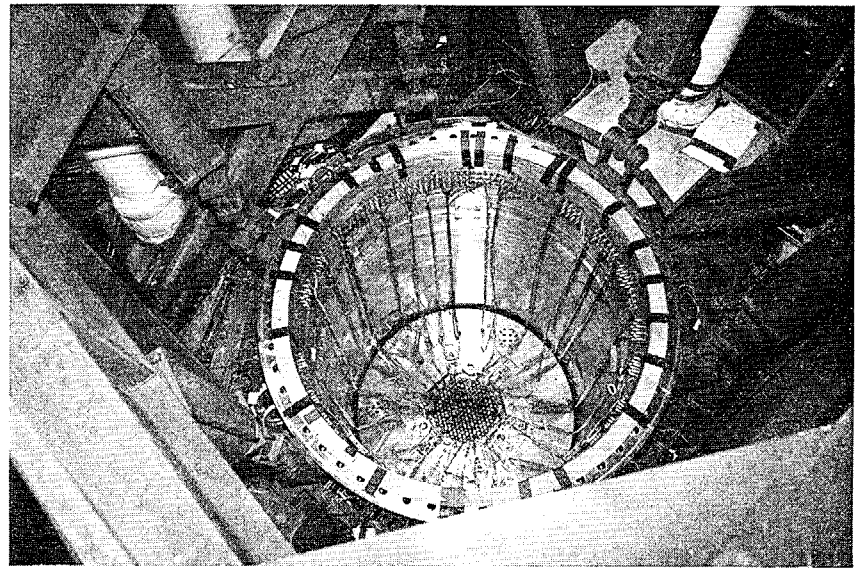

Figure 11. Core Assembly Installed

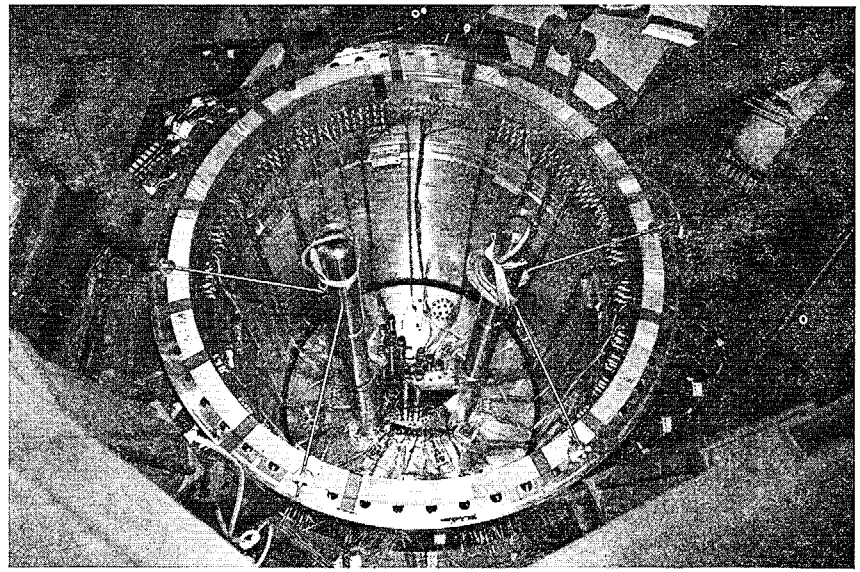

Figure 12. Instrument Tree Installation

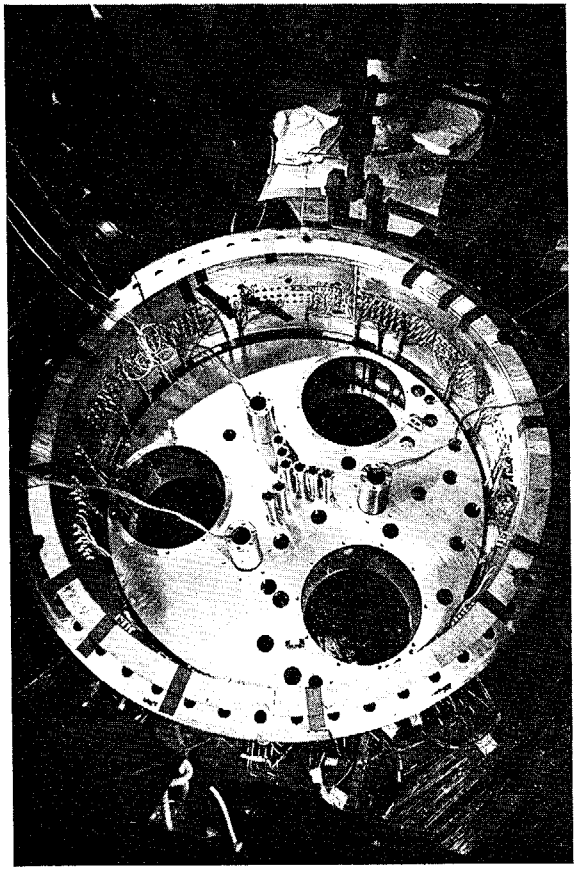

Figure 13. False Head Installation

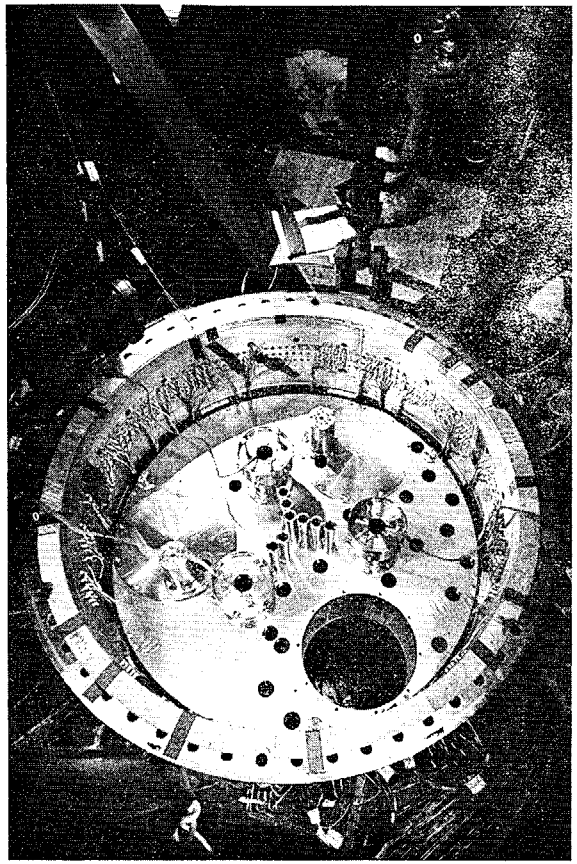

Figure 14. Installation of Head-Hung Components

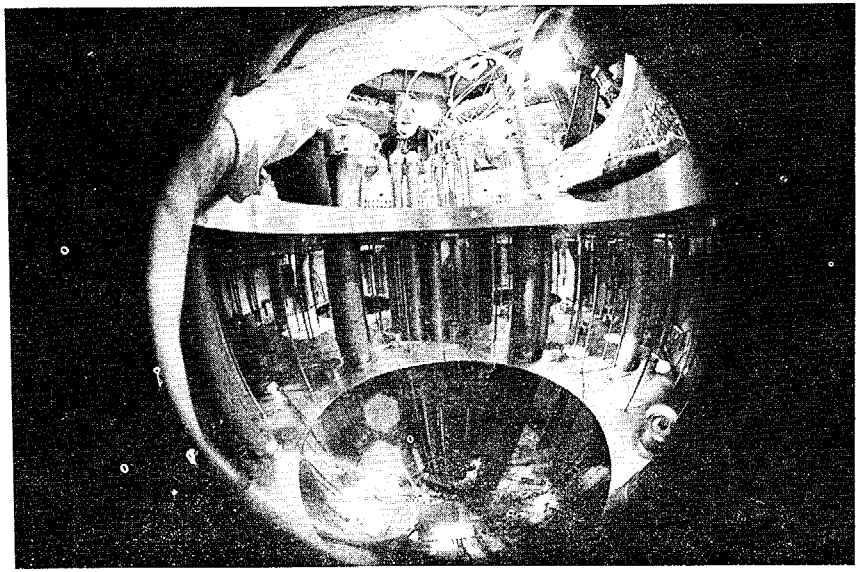

Figure 15. Interior View

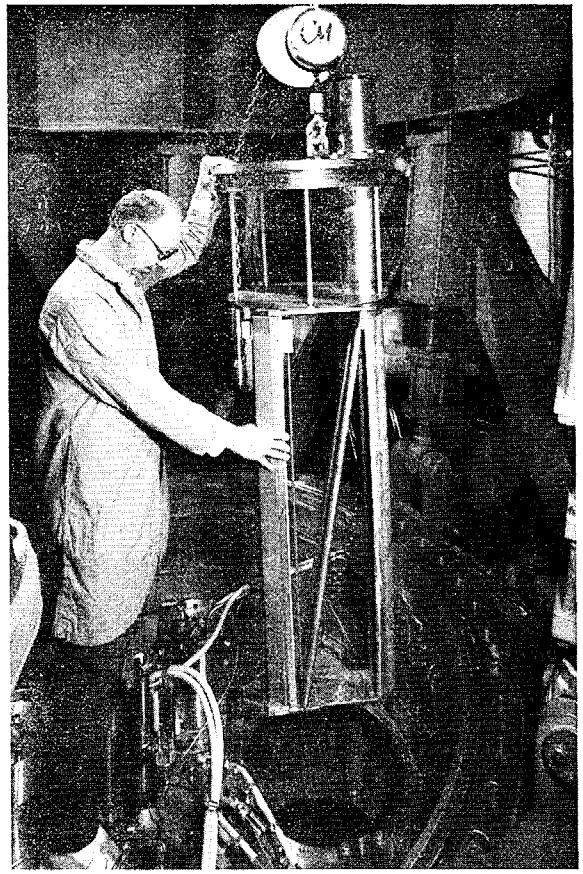

Figure 16. Installation of IVHM

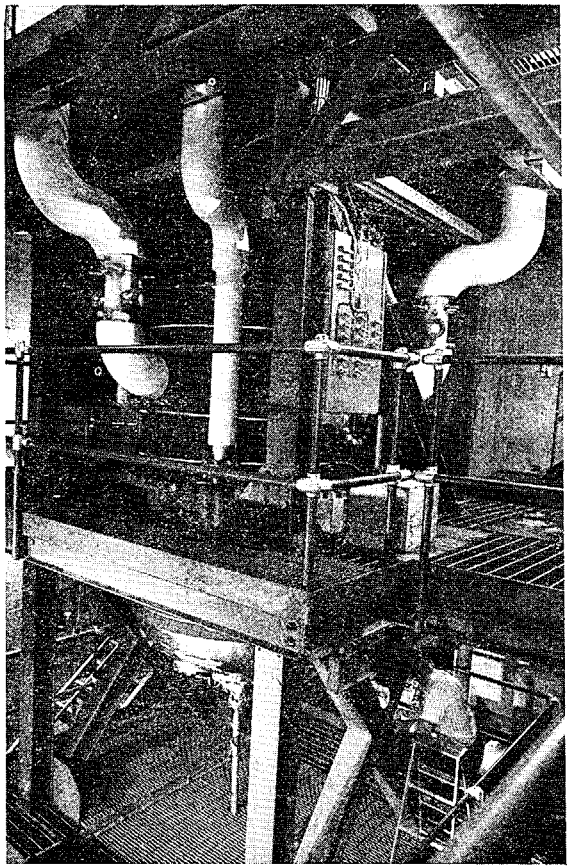

Figure 17. Overall View of Vessel

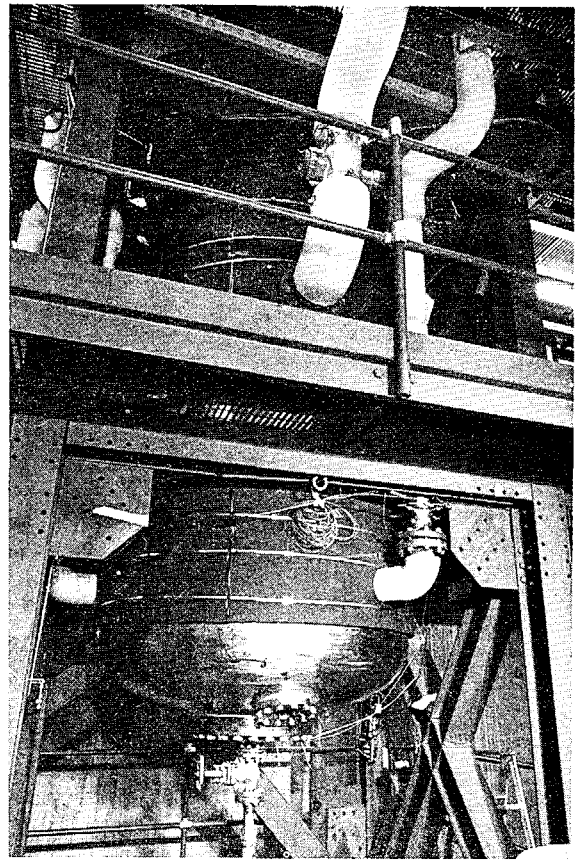

Figure 18. HCM Vessel

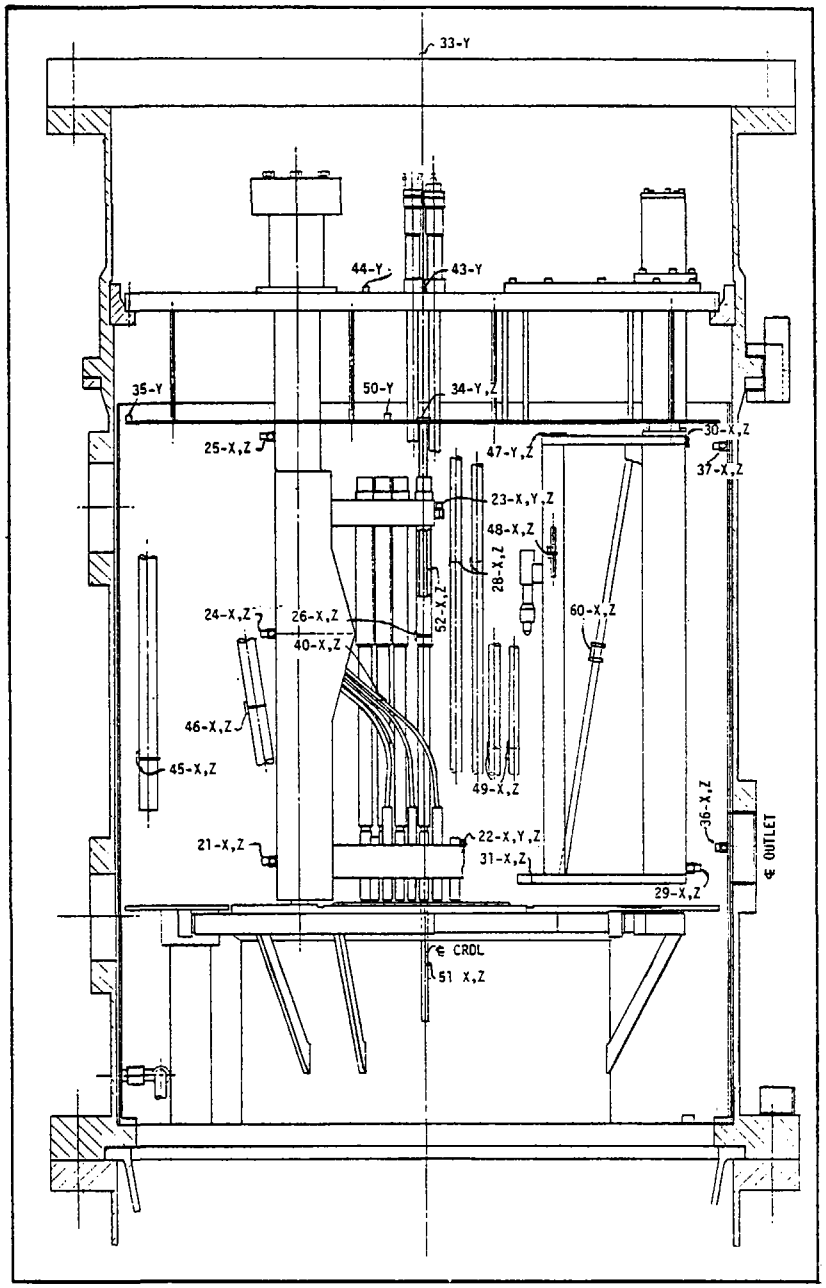

Figure 19a. HCM Accelerometer Location - Outlet Plenum

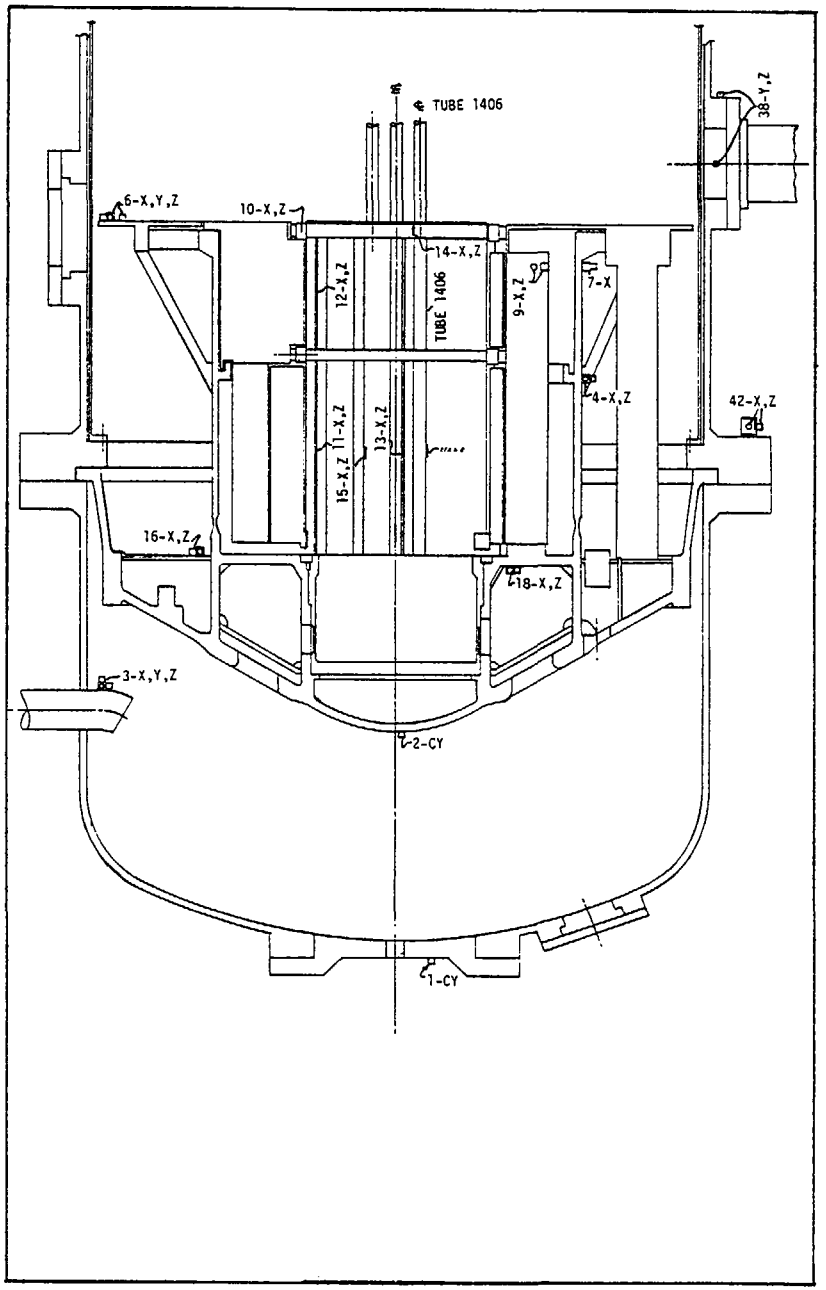

Figure 19b. HCM Accelerometer Location - Core

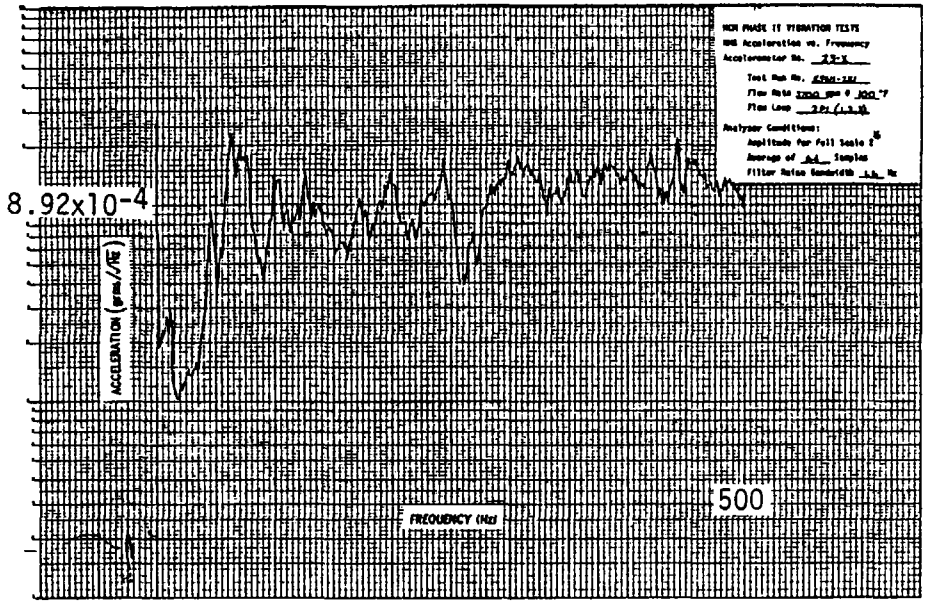

Figure 20. PSD - Instrument Tree (23X)

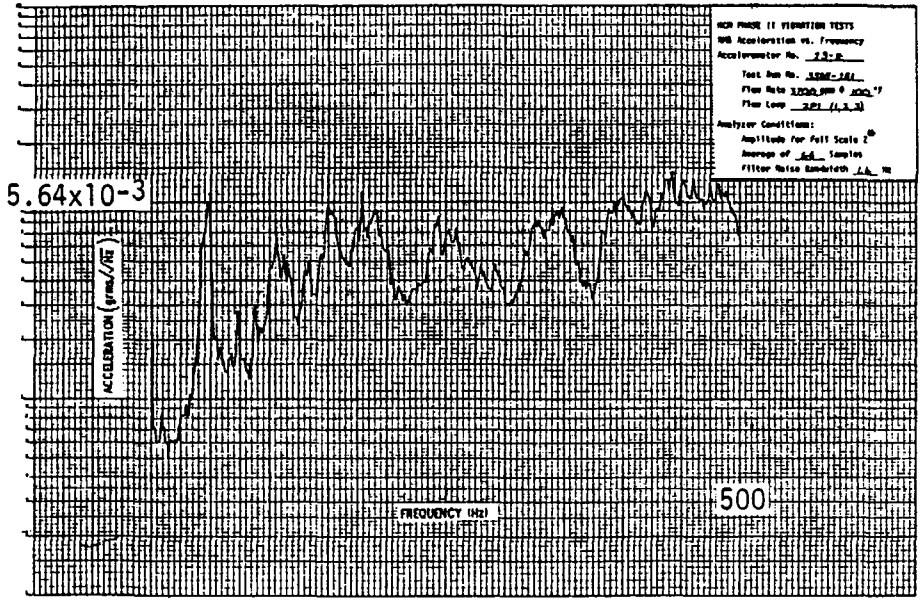

Figure 21. PSD - Instrument Tree (23Z)

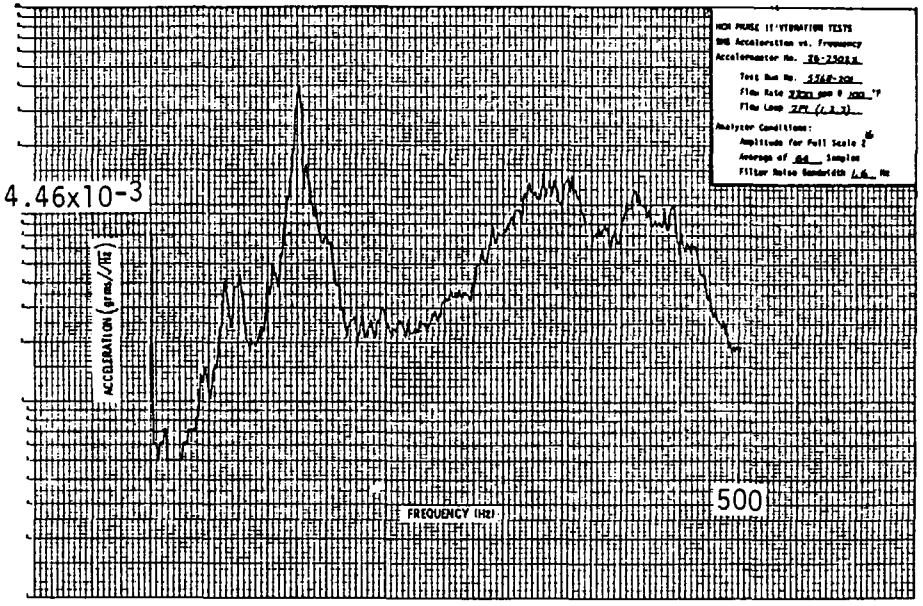

Figure 22. PSD - Control Rod Guide Tube (26-2502X)

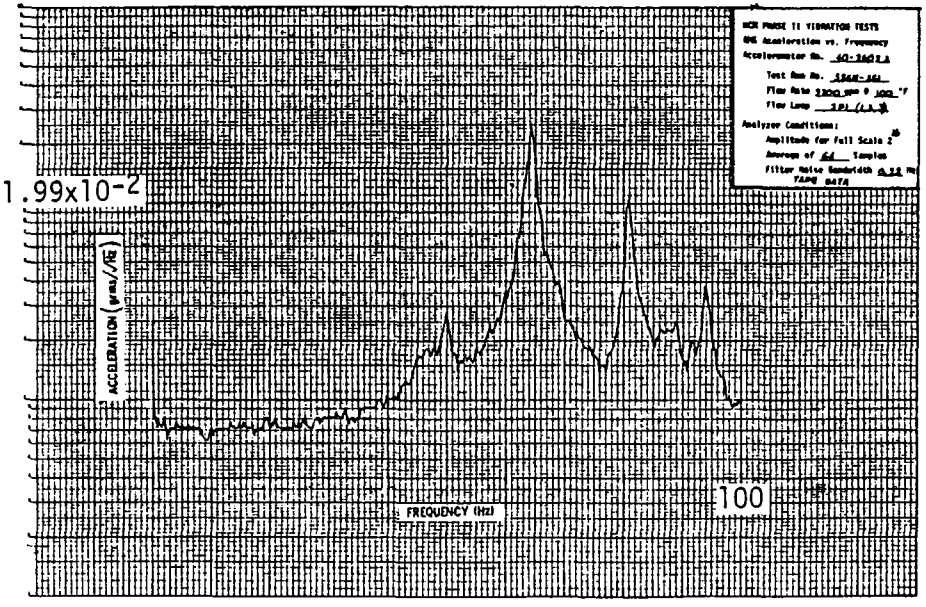

Figure 23. PSD - Instrumentation Guide Tube (40-2603X)

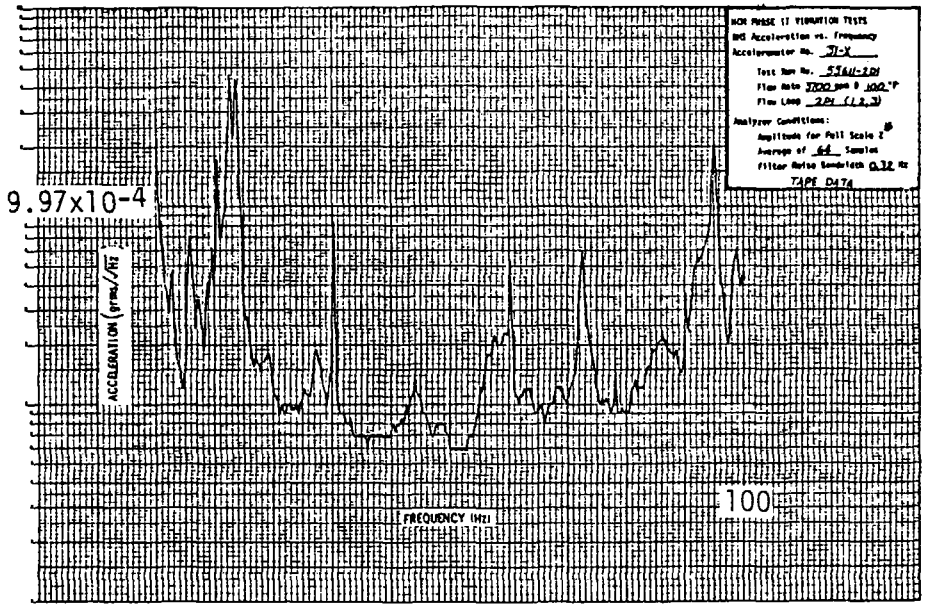

Figure 24. PSD - IVHM (31X)

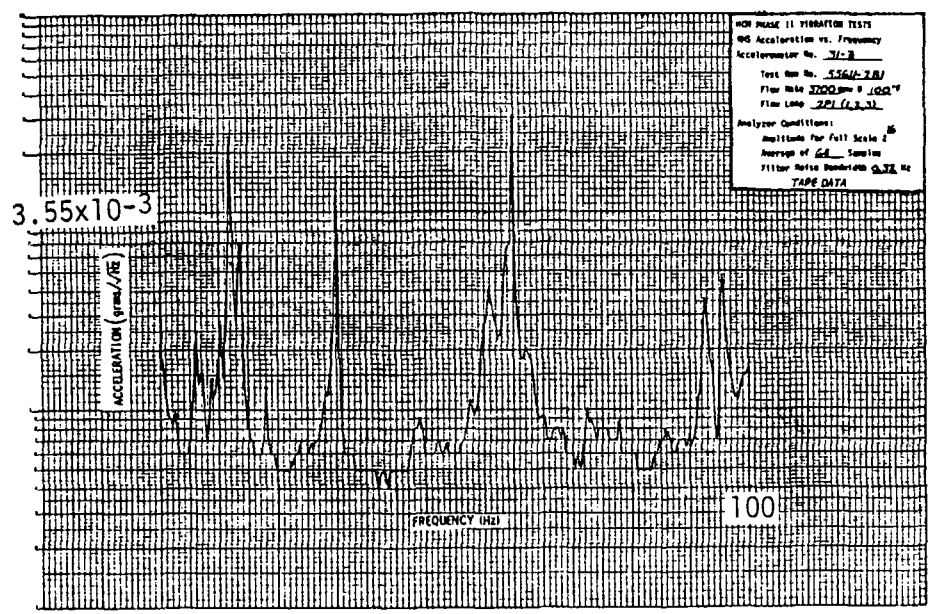

Figure 25. PSD - IVHM (31Z)

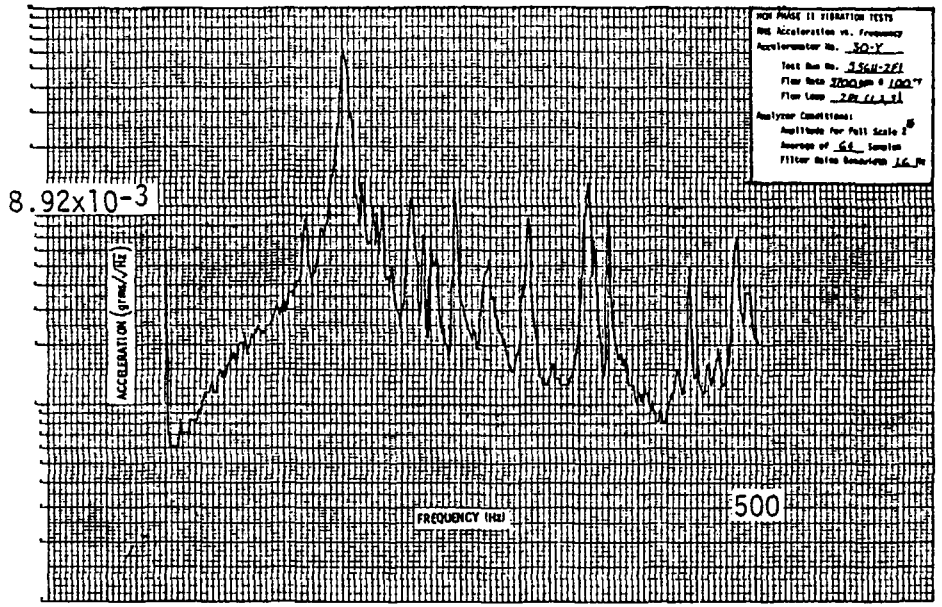

Figure 26. PSD - Vortex Suppressor Plate (50Y)

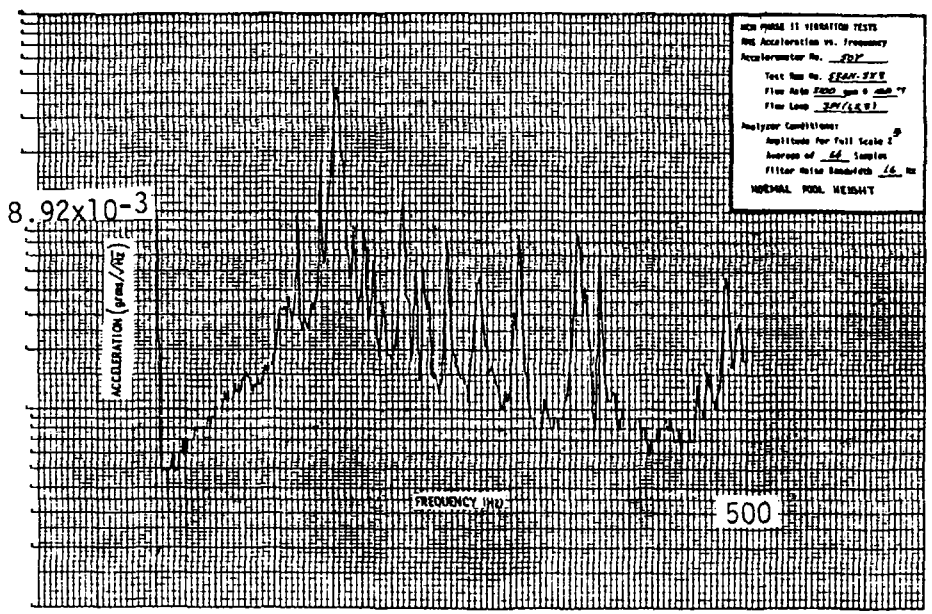

Figure 27. PSD - Vortex Suppressor Plate (50Y)
(Normal Pool Height)

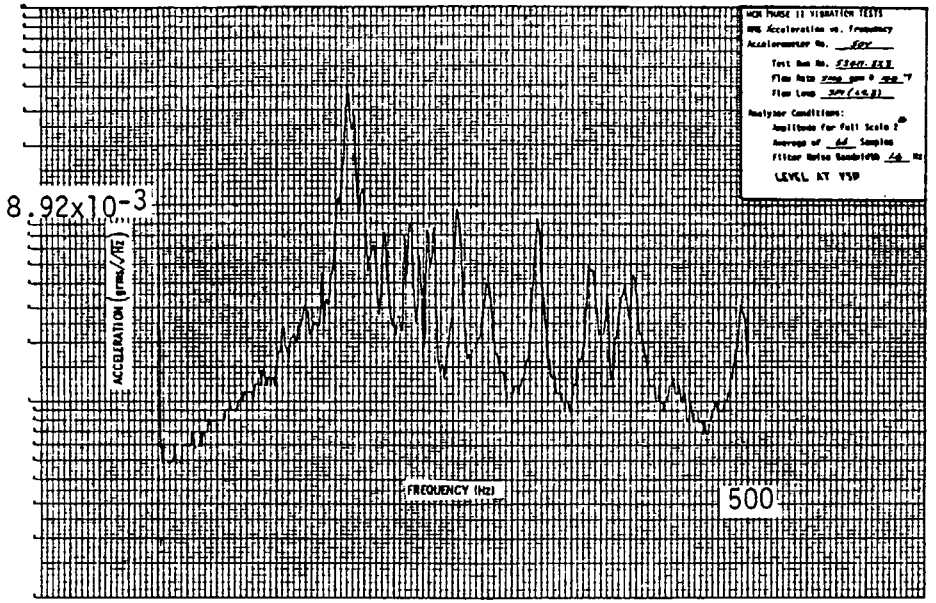

Figure 28. PSD - Vortex Suppressor Plate (50Y)
(Pool Level at VSP)

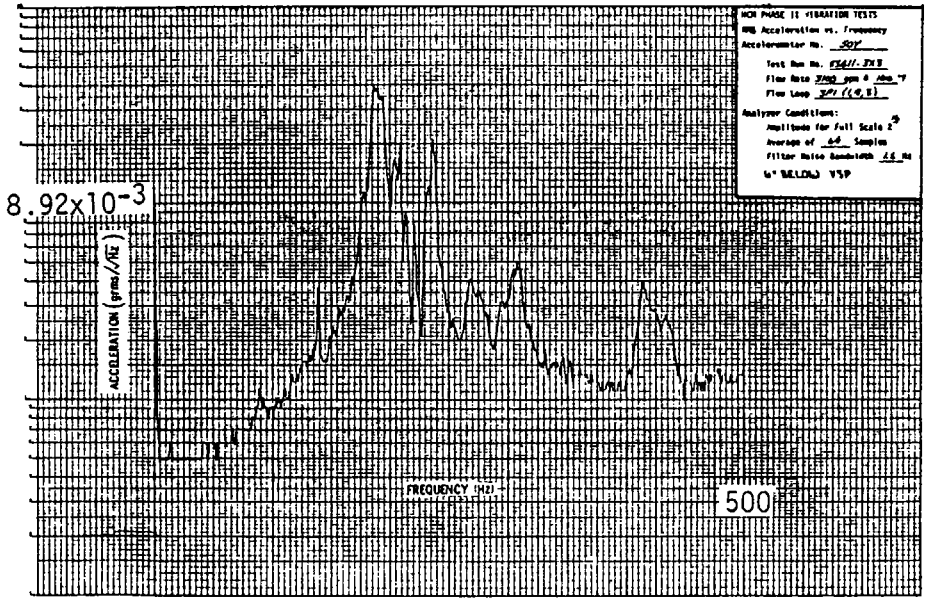

Figure 29. PSD - Vortex Suppressor Plate (50Y)
(Pool Level 6 Inches Below VSP)

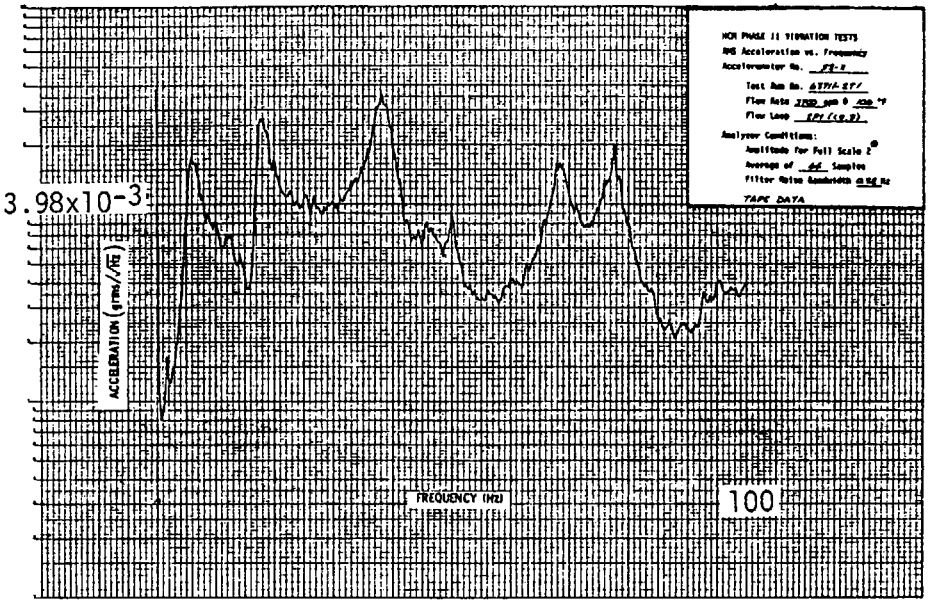

Figure 30. PSD - CRDL (52X)

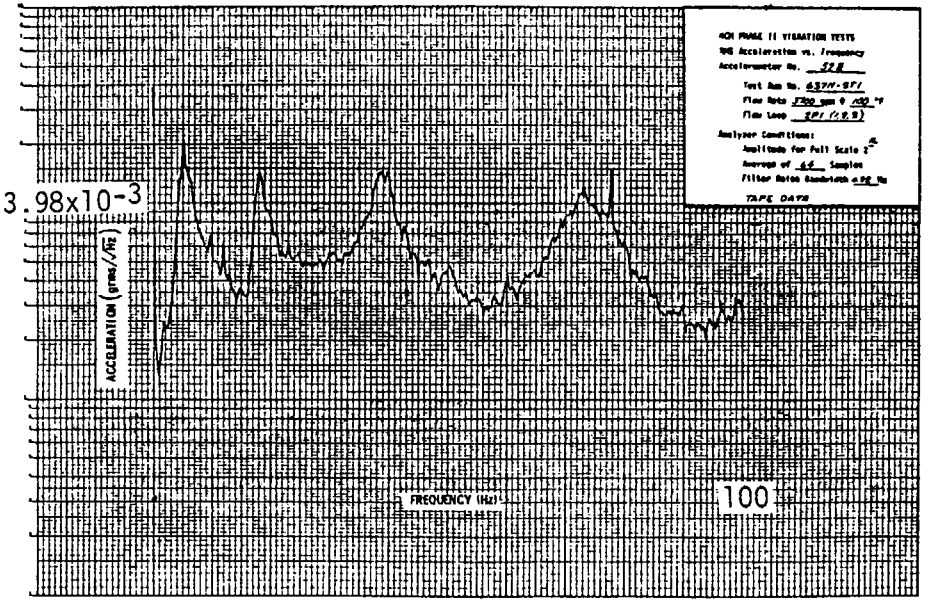

Figure 31. PSD - CRDL (52Z)

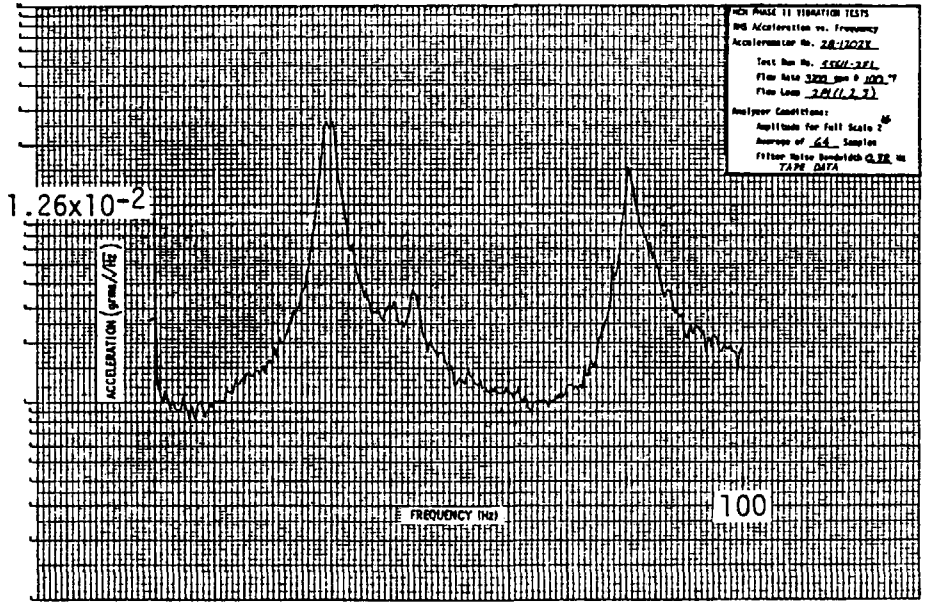

Figure 32. PSD - CLIRA (28-1202X)

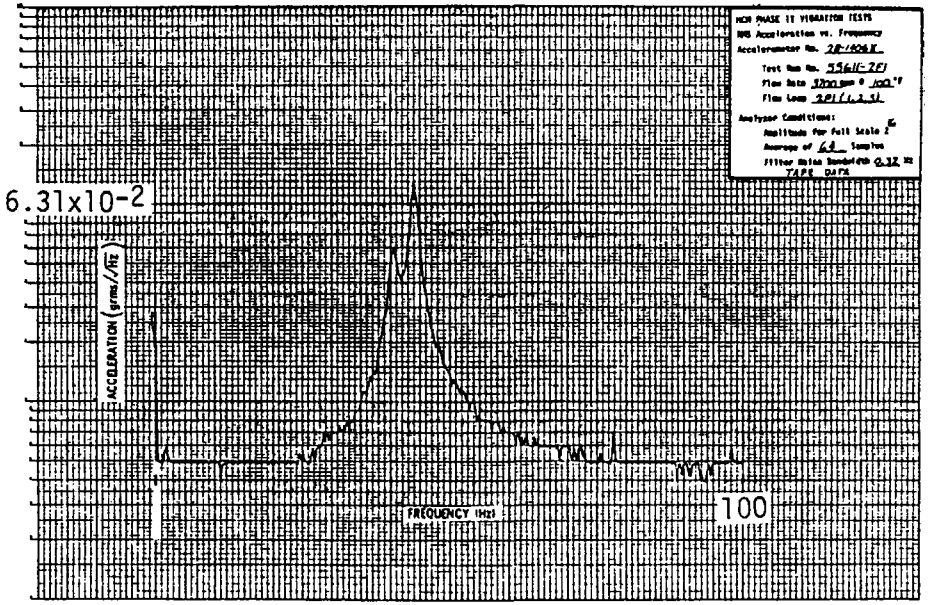

Figure 33. PSD - CLIRA (28-1406X)

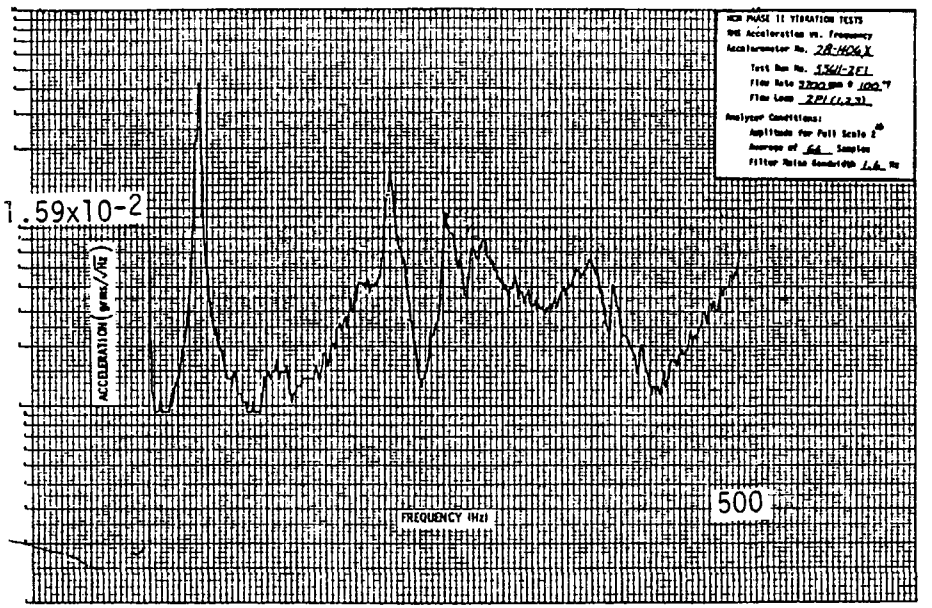

Figure 34. PSD - CLIRA (28-1406X)

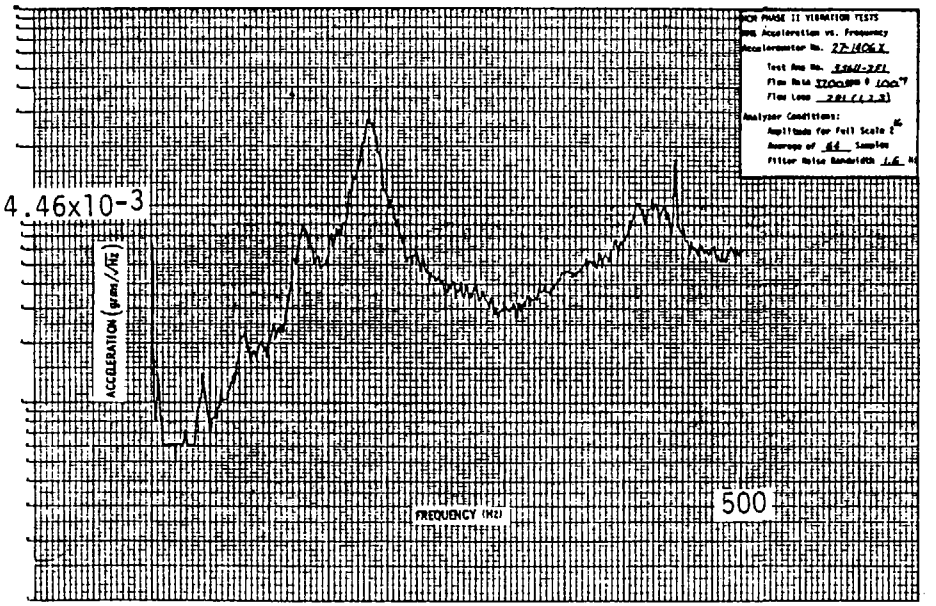

Figure 35. PSD - CLIRA (27-1406X)

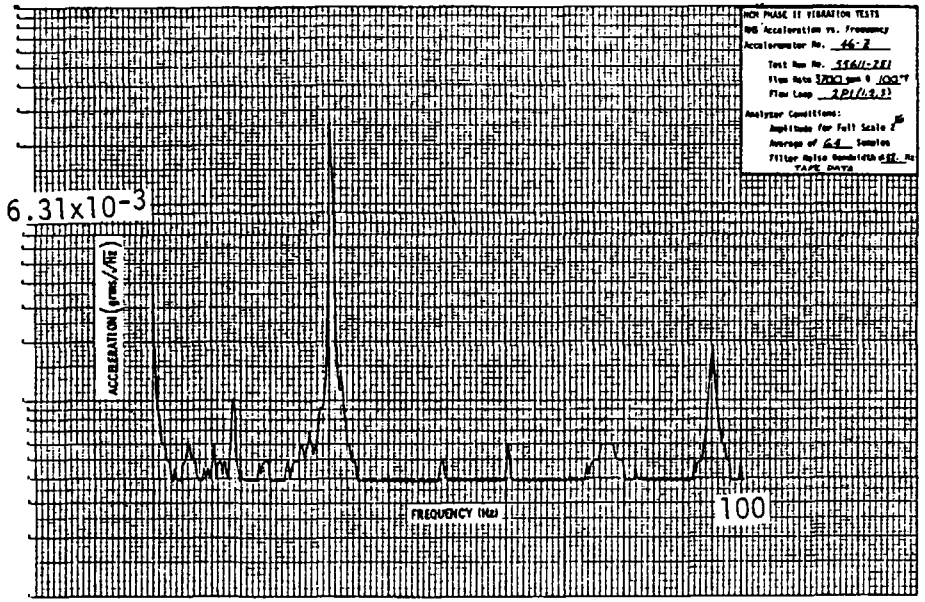

Figure 36. PSD - LLFM (46-Z)

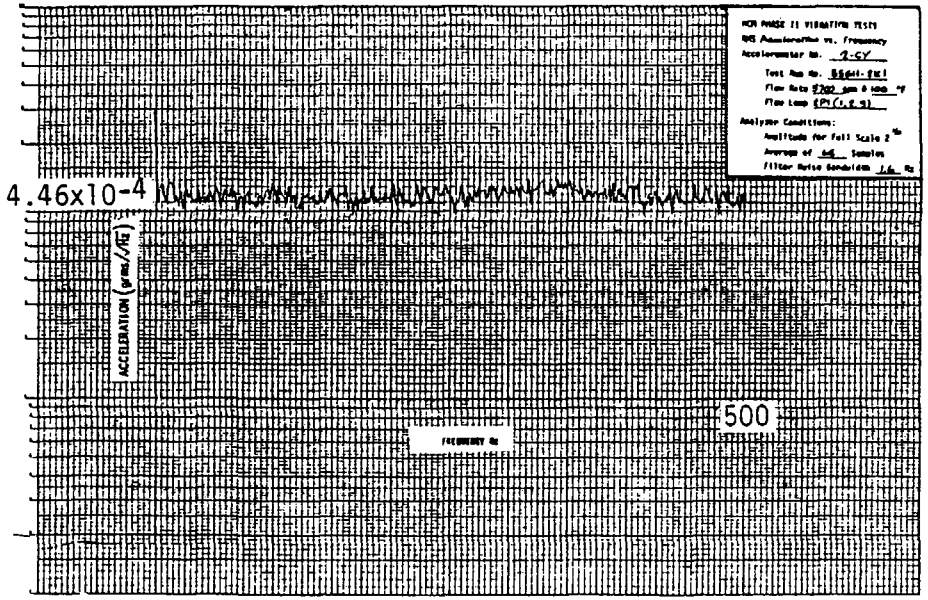

Figure 37. PSD - Core Support Structure (2CY)

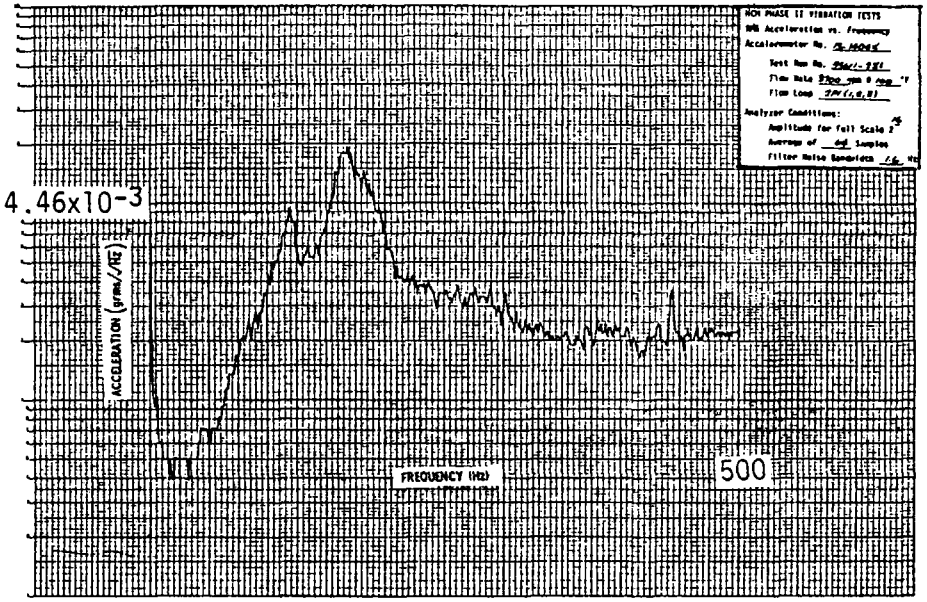

Figure 38. PSD - Driver Assembly (13-1404X)

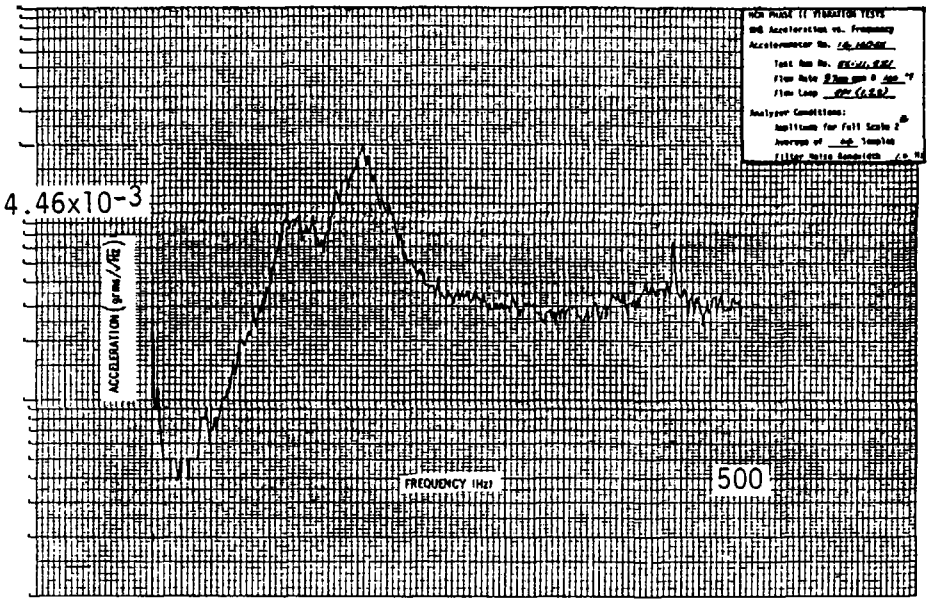

Figure 39. PSD - Driver Assembly (14-1404X)

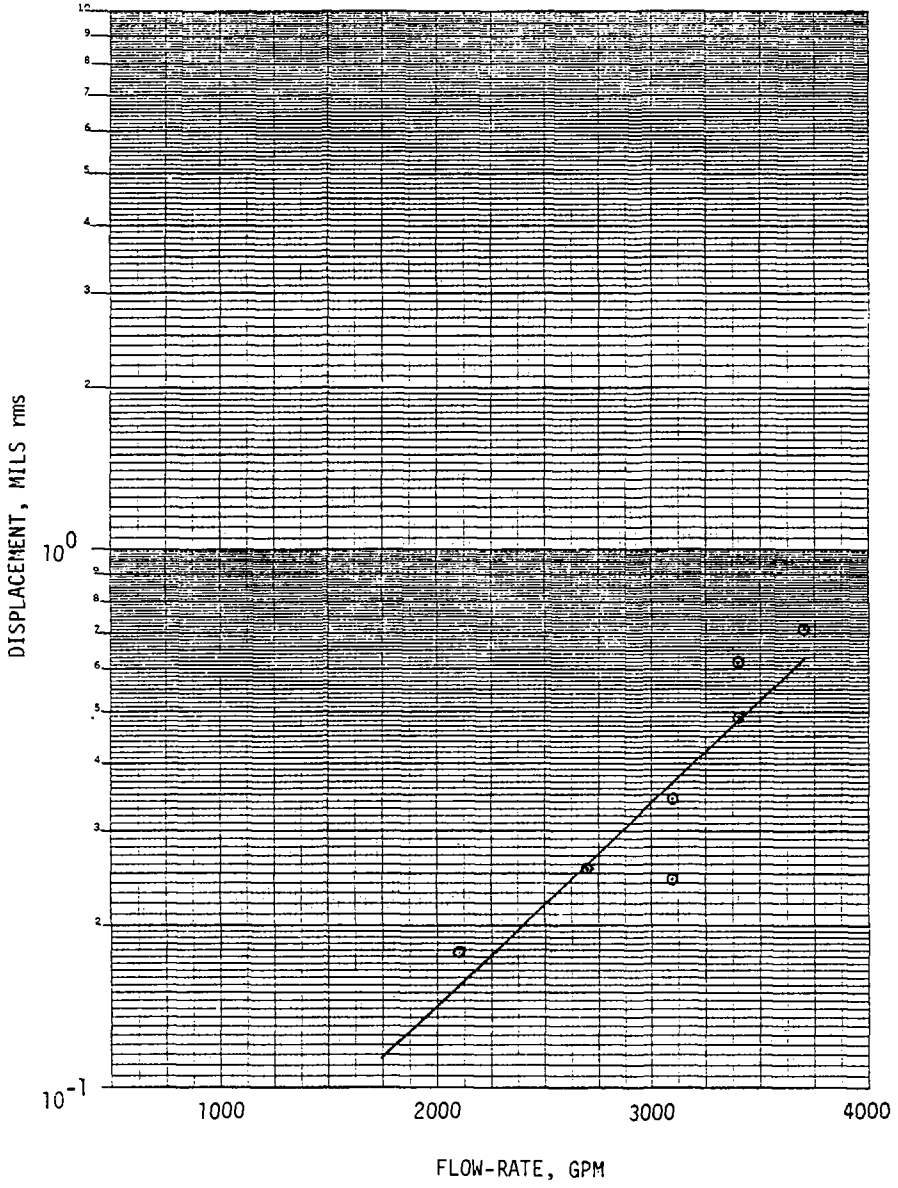

Figure 40. LLFM Displacement

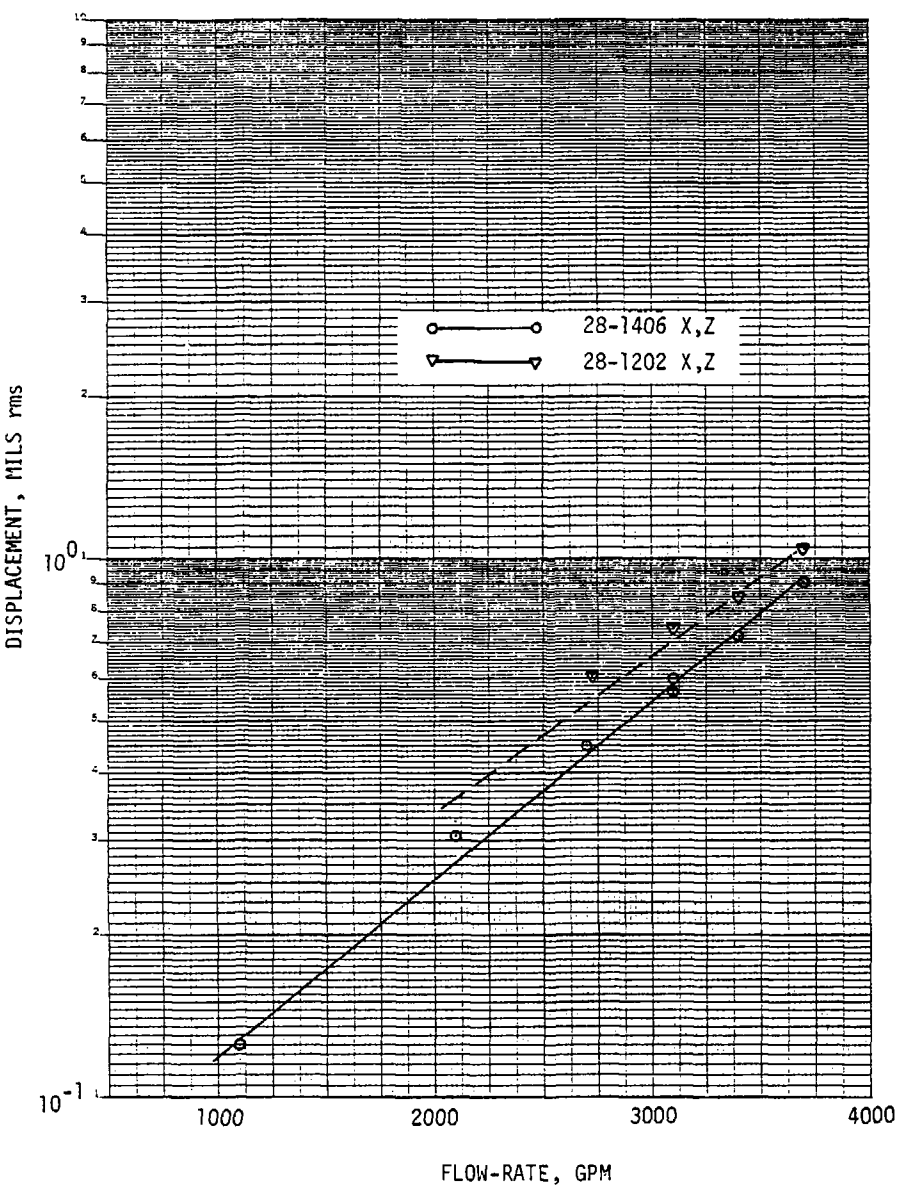

Figure 41. CLIRA Displacement

TABLE 1
HCM/PROTOTYPE PARAMETERS

PARAMETER	MODEL		PROTOTYPE	RATIO (Model)/(Prototype)		
	95°F	250°F	1050°F		95°F	250°F
E (lbs/in^2)	28×10^6	27.4×10^6	22.1×10^6	E_m/E_p	1.27	1.24
ρ_s (lbs/in^3) (Mat'l Density)	0.288	0.286	0.279	$(\rho_s)_m/(\rho_s)_p$	1.03	1.02
ρ (lbs/in^3) (Fluid Density)	0.036	0.034	0.027	ρ_m/ρ_p	1.33	1.26
ν (in^2/sec) (Kinematic Viscosity)	1.065×10^{-3}	3.799×10^{-4}	4.104×10^{-4}	ν_m/ν_p	2.59	0.93

TABLE 2
HCM/PROTOTYPE SCALING FACTORS

PARAMETER	TEMPERATURE	
	95°F	250°F
$\frac{\Delta_m}{\Delta_p}$ (Displacement)	0.285	0.285
$\frac{f_m}{f_p}$ (Frequency)	3.88	3.90
$\frac{\ddot{x}_m}{\ddot{x}_p}$ (Acceleration)	4.30	4.25
$\frac{F_m}{F_p}$ (Force)	0.103	0.101

TABLE 3
SUMMARY OF FTR VIBRATION RESULTS

COMPONENT	PRIMARY VIBRATION DESIGN CRITERIA	FREQUENCIES		TESTS		REMARKS
		FORCED f_s	FUNDAMENTAL f_o	EX-REACTOR	IN-REACTOR	
ABSORBER ASSY.	NONE	UNDEFINED	17	PROTOTYPE (HCM)	NO	LOW FREQUENCY OSCILLATIONS OF INNER ASSEMBLY WERE NEGLIGIBLE
CLIRA	VORTEX SHEDDING	3.3-5.0	9.5	HCM	NO	HCM $f_o \approx 11.5$ Hz: NO FLOW RESONANCES
CORE BARREL	NONE	18.9	32	HCM	NO	NO SIGNIFICANT HCM RESPONSE
CORE RESTRAINT	NONE	UNDEFINED	NOT CALCULATED	HCM	NO	HCM SIMULATED PASSIVE SYSTEM; RESP. NEGLIGIBLE
CRDM	VORTEX SHEDDING	6.3	1-30	HCM	NO	HCM REVEALED DASHPOT IMPACTING; ADJUDGED ACCEPT.
CSS	NONE	18.9	98-UP	HCM	NO	HCM SHOWED NEGLIGIBLE RESPONSE FROM 0-130 Hz; $f_o > 130$ Hz
FUEL ASSEMBLY	MAX. DISPL. < 2 MILS MIS	10-20	17-24	PROTO. (HCM)	NO	WATER TESTS SHOWED > 2 MILS RMS FOR LOOSE DUCT; N_a TEST SHOWED NO WEAR.
HOR. BAFFLE PLATES	VORTEX SHEDDING	1.0	93.5-96	HCM	NO	LOW AMPLITUDE RESPONSE
ICSA	NONE	UNDEFINED	NOT CALCULATED	NONE	NO	SIMILAR TO FUEL ASSY.
IT	VORTEX SHEDDING	MAIN FRAME 8.5 IGT 6.2-43	8.9 13	HCM & PROTO.	IGT	HCM IGT $f_o \approx 14.5$ Hz; RESPONSE LOW
IVHM	VORTEX SHEDDING	7.8-9.7	4.7-5.5	HCM	NO	NO SIGN. HCM RESPONSE; IVHM IN LOW FLOW REG.
IVSM	NONE	18.9	32	HCM	NO	NO MEAS. MADE ~ IN LOW FLOW REGIME
LLFM	VORTEX SHEDDING	1.1-1.7	1.6-8.0	HCM & PROTO.	DUMMY SENSOR.	HCM $f_o \simeq 8.0$ Hz; LOW RESPONSE
PIOTA	VORTEX SHEDDING	4.8	6.5	HCM	NO	HCM $f_o \simeq 11.1$ Hz; LOW RESPONSE
REFLECTORS	NONE	UNDEFINED	NOT CALCULATED	HCM	NO	NO SIGNIFICANT HCM RESPONSE
SHIELD ASSY.	VORTEX SHEDDING	1.2-3.4	23-127	HCM	NO	NO SIGNIFICANT HCM RESPONSE
THERMAL LINER	NONE	UNDEFINED	NOT CALCULATED	HCM	NO	HIGHLY DAMPED HCM RESPONSE
T/LLM	VORTEX SHEDDING	1.2-3.2	4.5	HCM	NO	NO SIGNIFICANT HCM RESPONSE
VOTA	TBD	4.8	TBD	ENGR. MODEL (HCM)	YES	VOTA TO BE PRINCIPAL TRANSDUCER FOR ATP PLUS FOLLOW-ON SURVEILLANCE
VSP	VORTEX SHEDDING	40.3	20-45	HCM	NO	HCM $f_o > 20$ Hz, ACCEPTABLE RESPSONSE

INSTRUMENT TREE NORMALIZED RESPONSE

TABLE 4

	ACCELEROMETER NUMBER									
FREQUENCY (Hz)	21X	21Z	22X	22Z	23X	23Z	24X	24Z	25X	25Z
47	0.46		0.27		1.00		0.65		0.70	
51		0.13		1.00		0.44		0.54		
64					1.00		0.72		0.83	
72	0.15		0.21		1.00		0.76		0.98	
101	0.52		0.32		1.00		0.54		0.94	
105		-0.30		0.10		1.00		-0.74		-0.73

IVHM NORMALIZED RESPONSE

TABLE 5

	ACCELEROMETER NUMBER						
FREQUENCY (Hz)	29X	29Z	30X	30Z	31X	31Z	47Z
12.5	1.00	0.35	0.05	0.04	0.42	-0.75	-0.16
13.8	1.00	0.14	0.04	0.02	0.04	-0.23	-0.33
29		1.00		0.22		-0.53	-0.11
59		-0.57		-0.13		1.00	-0.29
104	0.43	-0.21	1.00	0.32	0.25	-0.21	-0.30
123		-0.46		0.16		0.52	1.00
134	-0.16	1.00	0.27	0.84	0.16	0.12	-0.44

NORMALIZED INSTRUMENT TREE RESPONSE: FLOW TESTS/SHAKER TESTS

TABLE 6

	ACCELEROMETER NUMBER									
FREQUENCY (Hz)	21X	21Z	22X	22Z	23X	23Z	24X	24Z	25X	25Z
47 (49)	0.46 0.50		0.27 0.59		1.00 1.00		0.65 0.75		0.70 0.66	
51 (51)		0.13 0.15		1.00 --		0.44 1.00		0.54 0.47		-- 0.60
64 (65)	0.10		0.09		1.00 0.80		0.72 0.57		0.83 1.00	
72 (72)	0.15 0.17		0.21 0.14		1.00 1.00		0.76 0.85		0.98 0.96	
101 (106)	0.52 0.57		0.32 0.72		1.00 1.00		0.54 0.50		0.94 1.00	
105 (112)		-0.30 -0.20		0.10 0.09		1.00 1.00		-0.74 -0.70		-0.73 -0.87

NOTE: Shaker test frequency in parenthesis

NORMALIZED IVHM RESPONSE FLOW TEST/SHAKER TEST

TABLE 7

	ACCELEROMETER NUMBER						
FREQUENCY (Hz)	29X	29Z	30X	30Z	31X	31Z	47Z
12.5	1.00	0.35	0.05	0.04	0.42	-0.75	-0.16
13.8 (12.8)	1.00 1.00	0.14 0.11	0.04 --	0.02 0.06	0.40 0.29	-0.23 -0.21	-0.33 --
29 (30)	-0.08	1.00 -0.83		0.22 -0.83		-0.53 1.00	-0.11 0.25
59 (59)	-- 0.09	-0.57 -0.48	-- 0.14	-0.13 -0.48		1.00 1.00	-0.29 -0.81
104 (105)	0.43 0.75	-0.21 0.35	1.00 --	0.32 0.80	0.25 1.00	-0.21 0.20	-0.30 1.00
123 (125)	-- 0.07	-0.46 -0.20		0.16 0.21		0.52 0.42	1.00 1.00
134 (135)	-0.16 --	1.00 0.38	0.27 1.00	-0.84 -0.75	-0.16 --	0.12 0.06	-0.44 -0.70

NOTE: Shaker test frequency in parenthesis

HCM COMPONENT MODAL PARAMETERS (SHAKER TESTS) TABLE 8

COMPONENT	FREQUENCY (Hz)		MODE SHAPE	c/c_c	
	WET	DRY		WET	DRY
Instrument Tree	51	70	First mode: out-of-plane bending	5.5	4.0
Instrument Tree	65	77	First mode: in-plane bending	5.5	4.0
IVHM	12.8	14.5	First mode: in-plane bending	2.4	2.1
IVHM	30	34.2	First mode: torsion	1.4	1.5
LLFM	31	33	First mode: bending	1.9	2.7
CLIRA (1406)	44	65	First mode: bending	1.9	1.4